UHASSELT
KNOWLEDGE IN ACTION

Maastricht University

Faculty of Medicine and Life Sciences
School for Life Sciences
Master of Biomedical Sciences

Master's thesis

Human dental pulp stem cells as a potential carrier for the herpes simplex-1 virus thymidine kinase suicide gene for therapy of oral squamous cell carcinoma and characterization of the 4-nitroquinoline-1-oxide rat model

Leentje Rasking

Thesis presented in fulfillment of the requirements for the degree of Master of Biomedical Sciences, specialization Clinical Molecular Sciences

SUPERVISOR :
Prof. dr. Esther WOLFS

CO-SUPERVISOR :
Prof. dr. Annelies BRONCKAERS

2018
2019

Transnational University Limburg is a unique collaboration of two universities in two countries: the University of Hasselt and Maastricht University.

UHASSELT
KNOWLEDGE IN ACTION

www.uhasselt.be
Universiteit Hasselt
Campus Hasselt:
Martelarenlaan 42 | 3500 Hasselt
Campus Diepenbeek:
Agoralaan Gebouw D | 3590 Diepenbeek

UHASSELT
KNOWLEDGE IN ACTION

Maastricht University

Faculty of Medicine and Life Sciences
School for Life Sciences
Master of Biomedical Sciences

Master's thesis

Human dental pulp stem cells as a potential carrier for the herpes simplex-1 virus thymidine kinase suicide gene for therapy of oral squamous cell carcinoma and characterization of the 4-nitroquinoline-1-oxide rat model

Leentje Rasking

Thesis presented in fulfillment of the requirements for the degree of Master of Biomedical Sciences, specialization Clinical Molecular Sciences

SUPERVISOR :
Prof. dr. Esther WOLFS

CO-SUPERVISOR :
Prof. dr. Annelies BRONCKAERS

Acknowledgements

Ever since I lost my step-grandparents to the disease, I knew I wanted to contribute to cancer research and therapy. Thankfully, the Morphology research group of Hasselt University granted me the opportunity to intern in the cancer research field and combine this with the intriguing field of stem cell research. With this thesis, I complete an entire studious career, and throughout, I received aid from many people in many different forms.

First, I would like to thank my promotor, supervisor and confidant Prof. Dr. Esther Wolfs for granting me to opportunity to participate, learn and contribute to her research through this fascinating internship. Furthermore, I must thank her for so much more. The guidance but simultaneous freedom she granted me with designing my own experiments, the writing of this thesis and the fact that her door was always open when I ran into bumps along the road or wanted a talk, have made these eight months extraordinary. Even when bad news hit us, she encouraged me to start each day with great enthusiasm. A special thank you to Prof. Dr. Annelies Bronckaers, who was always up for a chat and had only encouraging words whenever I came into their office.

Moreover, I would like to thank the other members of the Morphology research group that I met; from help in the lab, to words of encouragement and constructive criticism, they have helped me grow and develop further as a scientist. A special thank you to Mrs. Jeanine Santermans and Mr. Marc Jans for their help in this project, and to Mrs. Petra Bex for all her help with the micro-injections and the delightful conversations between cells. Additionally, words cannot describe my gratitude for Olivier. Not only has he been an enjoyable lab partner during our cloning experiments; his presence elevated the work load and kept me sane throughout.

To everyone that shared our little office: you guys made this experience even more enjoyable. Thank you for the conversations, the 'sharing of facts' and the encouraging words when needed. I hope every one of you has a bright future ahead!

Furthermore, I want to thank Dr. Ir. Ilse Smets and Dr. Hannelore Bové. If not for them, I would have never considered transitioning from Biotechnology to Biomedical Sciences. Thank you for the little push that I did not know I needed.

Finally, I would like to my friends, especially Kenneth, Janne and Esme, for putting up with me, my whining and the reassuring words I needed; Thibaut, one lovely surprise I never expected to gain from this internship and my dad for every opportunity he ever granted me and for allowing and pushing me to aspire more in life.

Table of contents

List of abbreviations

^{124}I-FIAU	^{124}I-labeled 2'-fluoro-2'-deoxy-1β-darabinofuranosyl-5-[^{124}I]iodouracil
4NQO	4-nitroquinoline-1-oxide
BM-MSC(s)	Bone marrow-derived mesenchymal stem cell(s)
CD	Cluster of differentiation
CXCR-4	C-X-C chemokine receptor type 4
Cx-43	Connexin-43
Da	Dalton
DAB	3,3'-diaminobenzidine
DAPI	4',6-diamidino-2-fenylindool
DMEM/F12	Dulbecco's modified eagle medium nutrient mixture F12
DNA	Deoxyribonucleic acid
E. coli	*Escherichia coli*
EDTA	Ethylenediaminetetraacetic acid
EF1-α	Elongation factor 1-alpha
(e)GFP	(Enhanced) Green fluorescent protein
EGFR	Epidermal growth factor receptor
EpCAM	Epithelial cell adhesion molecule
FBS	Fetal bovine serum
fLuc	Firefly luciferase
FOXP3	Forkhead box P3
(3P-)GCV	(Triphosphorylated) Ganciclovir
GDEPT	Gene-directed enzyme prodrug therapy
GJIC	Gap junctional intercellular communication
hDPSC(s)	Human dental pulp stem cell(s)
HLA	Human leukocyte antigen
HPV	Human papilloma virus
HSV1-sr39-tk/TK	Herpes simplex virus 1-thymidine kinase gene/protein mutant s39
IL	Interleukin
IRES	Internal ribosomal entry site
Kb	Kilo bases
MAGEA	Melanoma-associated antigen
MEM	Minimal essential medium
MRI	Magnetic resonance imaging
NP(s)	Nanoparticle(s)
NSC(s)	Neural stem cell(s)
(O)SCC	(Oral) Squamous cell carcinoma
PBS	Phosphate buffered saline
PET	Positron emission tomography
PURO^{R}	Puromycin resistance gene
RNA	Ribonucleic acid
ROS	Reactive oxygen species
rpm	Rotations per minute
rSAP	Shrimp alkaline phosphatase
RT	Room temperature
SDF-1	Stromal cell-derived factor 1
T2A	Self-cleaving 2A peptide variant T
TAE	Tris acetic acid EDTA buffer
TGF	Transforming growth factor
TK	Thymidine kinase
TNF	Tumor necrosis factor
UM-SCC-14C	University of Michigan-squamous cell carcinoma-14C
VEGF	Vascular endothelial growth factor

Summary

Introduction. In 2018, 2.5% of all cancers could be attributed to oral cancer. Over 90% of these oral cancers belong to the class of oral squamous cell carcinoma (OSCC), which are malignancies that originate from the oral cavity and oropharynx. The survival rates have been consistent in recent decades despite numerous advances in research and therapy. Surgical resection of the oral floor or tongue leads to complications in mastication, speech and altered aesthetics. Furthermore, radio- and chemotherapy hold a high risk of tumor recurrence and adverse effects such as xerostomia.

The herpes simplex virus 1-thymidine kinase (HSV1-tk) mechanism is proposed to address these side effects. Transduction of cells with the HSV1-tk suicide gene renders the cells capable to modify ganciclovir, metabolically trapping it and leading to apoptosis. To date, lentiviral vectors are used to introduce the transgene into cancer cells; however, these vectors are a suboptimal delivery system associated with safety issues. Cellular vehicles such as human dental pulp stem cells (hDPSCs) could address these issues. Human DPSCs are a subtype of mesenchymal stem cells which are known to migrate to tumorous tissue and hence, can be an ideal candidate to carry the suicide gene to the tumor. Additionally, the mutant HSV1-sr39-tk holds a higher efficiency towards ganciclovir (GCV). Therefore, we hypothesized that therapy with HSV1-sr39-tk$^+$ hDPSCs results in the death of OSCC cells through the bystander effect and elicits a subsequent reduction of tumor size.

Materials and Methods. First, the HSV1-sr39-tk gene and firefly luciferase (fLuc) gene were introduced into a plasmid harboring the elongation factor 1-alpha promotor and a puromycin resistance cassette. The control plasmid contains green fluorescent protein (eGFP) instead of the suicide transgene. Gap junction formation and functionality were assessed through a connexin-43 staining and Lucifer Yellow dye coupling in a co-culture of hDPSCs and OSCC cells, respectively. Furthermore, the 4-nitroquinoline-1-oxide (4NQO) rat model was optimized. 4NQO was administered topically onto the tongue surface or added to the drinking water. Animals were exposed for 1 – 9 months and the tumor formation and development were evaluated *ex vivo* through (immuno)histochemical analysis. Tongue sections were evaluated with the Masson's trichrome staining and antibodies against p63, CD44 and MAGEA-3/4.

Results and Discussion. HSV1-sr39-tk is successfully introduced into a plasmid; however, the control plasmid has not yet been finished due to an additional fragment in the samples. Gap junction presence is confirmed via a connexin-43 staining and the dye coupling evaluation demonstrates functional gap junctions and additionally indicates a connected cell network through gap junctions. Rats exposed to 4NQO ad libitum show a gradual transition from dysplasia to OSCC confirmed by immunostaining while topically administered rats ceased similar tumor growth. Until five months of 4NQO exposure little tumorous tissue is detected. However, after eight months invasion into the connective tissue and keratin pearl formation can be distinguished.

Conclusion. Gap junction presence and functionality were elucidated, confirming an important pillar of HSV1-tk suicide gene therapy. (Immuno)histochemical analysis of the 4NQO rat model indicates the optimal therapeutic window for *in vivo* studies after 6 – 7 months of 4NQO ad libitum. Both vectors must be generated before optimal GCV dosage can be determined *in vitro* to validate the HSV1-sr39-tk$^+$ hDPSCs as a carrier in suicide gene therapy as a therapeutic approach for OSCC.

1 Introduction

Cancer is the second leading cause of death worldwide and was responsible for an estimated 9.6 million deaths in 2018 (1). All multicellular animals can develop cancer, which is an abnormal unrestricted growth of cells. These cells carry the potential to invade or spread to other parts of the body other than their primary appearance. Moreover, all tumor cells portray the six hallmarks of cancer: cell growth and division without the proper signals, continuous growth and division when contrary signals are given, avoidance of apoptosis, limitless number of cell divisions, promotion of blood vessel construction and invasion of tissue and formation of metastases (2).

In 2018, 2.5% of all cancers could be attributed to oral cancer (3). Oral cancer is a growing global health problem that is listed as one of the top ten most common cancers worldwide with a high mortality (4). Generally, oral cancer appearance and its mortality are due to both individual predisposition as well as exposure to carcinogens such as tobacco use, heavy alcohol intake and dietary habits (5). However, human papilloma virus (HPV) infections have also been strongly associated with oral cancer development (6).

1.1 Oral squamous cell carcinoma: a worldwide health issue

Over 90% of these oral cancers consist of oral squamous cell carcinomas (OSCC) (Figure 1; (7)), which are diverse malignancies that originate from the oral cavity and oropharynx (8). Squamous cells are flat, scale-like epithelial cells that have a high number of junctions (9). Squamous cell carcinoma (SCC) can arise anywhere in the oral cavity; however, most frequent locations include the ventral surface of the tongue, the floor of the mouth, the lower lip, the soft palate and the gingiva (7).

OSCC more frequently affects man than women, probably due to higher exposure rates to e.g., tobacco or alcohol. The probability of OSCC development increases when persons are more exposed to the risk factors and increasing age also assists to mutagenic and epigenetic changes (10).

In some Western European countries such as Belgium an upward trend in OSCC incidence is observed (11). OSCC implies significant mortality and morbidity rates and despite numerous advances in research and therapy, the early stages of oral cancer go almost completely unnoticed and the mortality rates remain unchanged (4, 11). Consequently, the survival rates for oral cancer are among the lowest and continue to be consistent in recent decades leading to an average five-year survival rate of only 50% (4).

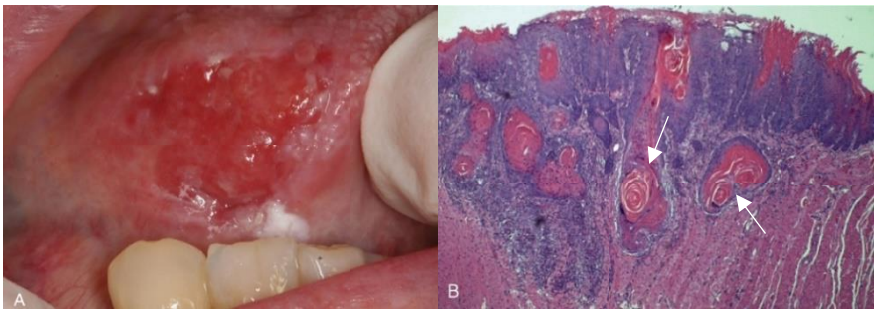

Figure 1 Proliferative and neoplastic lesions of the oral cavity: oral squamous cell carcinoma. *Figure* ***A)*** *depicts the clinical appearance of an ulceration and induration of the oral mucosa.* ***B)*** *depicts the histological appearance which demonstrates numerous nests and islands of malignant keratinocytes (white arrows) that invade the underlying connective tissue stroma.*

1.1.1 General treatment methodology

Current treatment strategies consist of surgical removal, radiotherapy, chemotherapy or a combination. Surgical resection relies on the adequate clearance of the tumor tissue, as inadequate clearance results in an increased risk of local and regional recurrence (12). However, when large parts of the oral floor and/or tongue are resected reconstructive surgery is required. Furthermore, complications in mastication and speech can occur and aesthetics can be altered (4, 12). Post-surgery, radiotherapy or simultaneous chemoradiotherapy is advised (12). Meanwhile, chemo- and radiotherapy hold a high risk of tumor recurrence and therapy-induced xerostomia (13). Therefore, the impact of oral cancer even after treatment results in severely reduced quality of life for survivors (4). Accordingly, finding and developing new treatment strategies that hold less severe side effects are crucial for the long-term survival and quality of life of patients with OSCC.

1.2 The herpes simplex virus 1-thymidine kinase mechanism

Suicide gene therapy is based on the principle of gene-directed enzyme prodrug therapy (GDEPT) and holds a great promise as a potential therapeutic approach (14). It implies the expression of a gene that encodes for a prodrug-activating enzyme. This enzyme is then introduced into the cancerous cells. The non-toxic prodrug is administered to the suicide gene-expressing cancer cells. This prodrug then becomes activated through phosphorylation by the suicide gene and leads to the formation of cytotoxic metabolites. These metabolites are trapped inside the cell and cause the induction of apoptotic pathways (14, 15). Various GDEPTs have been studied such as the cytosine deaminase gene of *Escherichia coli* (*E. coli)* that converts the prodrug 5-fluorocytosine to 5-fluorouracil or the herpes simplex virus 1-thymidine kinase gene (HSV1-tk) that converts its prodrug ganciclovir (GCV) to an intermediate monophosphorylated molecule. They rely on the host cell's enzymes to activate the prodrug through further di- and triphosphorylation (15). However, the HSV1-tk/GCV mechanism is the best characterized GDEPT.

Additionally, HSV1-tk also functions as an imaging reporter gene allowing the monitoring of the therapeutic effect *in vivo* through positron emission tomography (PET) (16). This form of non-invasive imaging requires a reporter gene (the HSV1-tk transgene that is expressed) but also a reporter probe that is converted by the enzyme into a trapped metabolite. The only reporter probes available for non-invasive imaging are radioactive tracers (16, 17). The radioactive tracer is a chemical compound where one or more atoms have been replaced by a radionuclide such as the ^{124}I-labeled 2'-fluoro-2'-deoxy-1β-darabinofuranosyl-5-[^{124}I]iodouracil (^{124}I-FIAU). The thymidine kinase enzyme phosphorylates the tracer and it gets trapped inside the cell due to its inability to pass the plasma membrane (18).

The HSV1-tk suicide gene is inserted into a lentiviral vector that is introduced into cancer cells (Figure 2). After transduction, these cancer cells express the viral protein thymidine kinase (TK), which can selectively monophosphorylate GCV. Ganciclovir is an antiviral drug that is used to treat infections associated with the cytomegalovirus (19) and is employed in this therapy as a non-toxic prodrug that is periodically administered to the HSV1-tk-expressing cancer cells (14). Viral TK will monophosphorylate the prodrug GCV and further di- and triphosphorylation is carried out by endogenous cellular kinases that are present inside the cancerous host cell. The triphosphorylated

form of GCV (3P-GCV) is highly toxic and gets metabolically trapped inside the host cell (14, 15) due to the negative charge that is created by its triphosphorylation. This purine analog inhibits deoxyribonucleic acid (DNA) polymerase, because it competes with the triphosphorylated substrate for the enzyme. Ultimately, DNA polymerase is stalled leading to the termination of nuclear and mitochondrial DNA synthesis. This initiates apoptotic pathways in the HSV1-tk-expressing cancer cells (14).

In addition, research has shown that these cancer cells form gap junctions; they are important for gap junctional intracellular communication (GJIC) and tumorigenesis (20-22). Even though the 3P-GCV cannot diffuse through the plasma membrane, it can migrate through these gap junctions to adjacent cells. This migration leads to the induction of apoptotic pathways in cancer cells that do not express the HSV1-tk suicide gene and thus, cannot convert GCV. This phenomenon is known as the bystander effect and will lead to an amplified toxic effect of suicide gene therapy (14, 15).

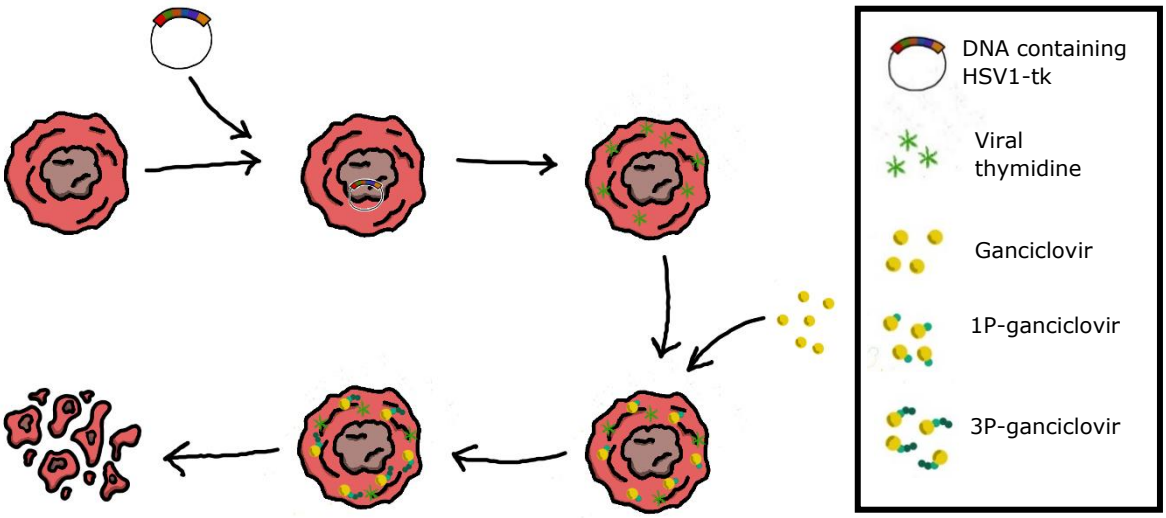

Figure 2 Overview of the HSV1-tk/GCV mechanism. *The viral vector that contains the HSV1-tk suicide gene is inserted into the cancer cell. After uptake into the genome, this cancer cell expresses the viral thymidine kinase protein. This protein can monophosphorylate the non-toxic prodrug ganciclovir and further phosphorylation by endogenous cellular kinases leads to a triphosphorylated, toxic form of ganciclovir (3P-GCV). 3P-GCV is incorporated into the cellular DNA leading to chain termination and apoptosis. Abbreviations: HSV1-tk, herpes simplex virus-1 thymidine kinase; 3P-GCV, triphosphorylated ganciclovir; DNA, deoxyribonucleic acid.*

1.2.1 Drawbacks of the herpes simplex virus 1-thymidine kinase mechanism

To date, this suicide gene therapy has demonstrated limited clinical efficacy mainly due to current gene delivery systems (23). Viral vectors show concerns about safety as well as targetability (24). A restricted spatial distribution of gene transfer vectors is observed as well as a poor gene transfer efficiency into cancer cells *in vivo* (25). Furthermore, by using gap junctions to create an amplified toxic effect suicide gene therapy is dependent on the amount of gap junctions formed between adjacent cancer cells. Additionally, the wildtype HSV1-tk gene displays a lower affinity for GCV. Therefore, the mutant form HSV1-sr39-tk that was generated by Gambhir *et al.* can address this issue. Cells expressing the mutant HSV1-sr39-tk suicide gene show an accumulated increase of substrates (such as GCV) by a factor 2.0 in comparison to cells that express the wild-type HSV1-tk (26).

1.3 Viral vectors to transfer the HSV1-tk suicide gene

Up until now in suicide gene therapy, the transgene is delivered to the site of interest by viral vectors. A viral vector is a recombinant viral particle where all excessive viral sequences of the original virus are deleted making it less pathogenic and replication incompetent. The HSV1-tk suicide transgene is added and this viral vector is introduced into the cancer cells. Through transduction, the viral particle introduces its genetic material into the host cell DNA leading to the expression of the viral thymidine kinase protein (27).

Several classes of viral vectors (i.e., lentiviral, retroviral and adenoviral vectors) have been employed in suicide gene therapy (27). These vectors are currently the elementary option to introduce the HSV1-tk suicide gene. However, they are also associated with safety issues as recombination can activate oncogenes or inactivate tumor suppressor genes or can reconstitute a replication competent and pathogenic virus (28). The issue with current viral delivery systems is that the expression of targeted proteins or receptors is not limited to cancer cells solely and that they are found routinely in normal, healthy cells (24). Other safety concerns include those that can lead to genotoxic events such as inflammation, insertional mutagenesis and disruption of normal genes that can lead to silencing of genes or oncogenesis (28, 29).

1.4 Vehicles to carry the suicide gene

The use of viral vectors as a gene delivery system is the major limiting factor in current cancer gene therapy (24). Therefore, a safe vehicle that carries the genetic material to the site of pathology is necessary. Other vehicles such as nanoparticles, liposomes or various cell types have been investigated as a potential way to introduce the suicide gene into the cancer cells (24, 30). The ideal vehicle would possess following crucial properties: the vehicle should be able to deliver the plasmid containing the suicide gene to specific cells, it should be stable and resist metabolic degradation until uptake and should allow the regulated expression of the suicide gene. Most importantly, the vehicle should be safe and should elicit the minimal amount of side effects in the human body (30).

1.4.1 Nanoparticles

Nanoparticles (NPs) are particles of 1 – 100 nanometer surrounded by an interfacial layer that is important for the required properties to deliver the suicide gene. A common feature is their large surface area to volume ratio (31, 32). Due to their cationic surface charge they have the ability to diffuse within the tumor tissue through passive transportation (33); this is possible due to the increased permeability that is observed in tumor vessels (15). Their biological and physicochemical properties such as shape, size and surface charge can be altered to the need of the therapy allowing them to bring the plasmid DNA to the cancer cell. However, these NPs are limited by the leakiness of the tumor vessels, which vary by cancer type and tumor size; this leads to toxicity in non-target tissues before the drug concentration can reach a therapeutic levels (32).

1.4.2 Biological vehicles

Biological vehicles are a potential therapeutic approach for suicide gene delivery. Microorganisms such as the commensal bacteria in the gut evade the host's immune responses, or exosomes can be exploited for suicide gene therapy (34). Bacteria such as modified *E. coli* are currently investigated (34, 35). Their cellular entry occurs through endocytosis into the cytoplasm where the transgene product can be expressed. These bacteria will produce ribonucleic acid (RNA) that efficiently acts as an expression cassette within the host cells (34). However, transgene expression levels when using bacteria are generally low compared to other delivery methods and their intrinsic toxicity is considered the most significant risk (34, 35).

Liposomes are phospholipid-based spherical particles that are derived from human cells. For example, exosomes are small membrane-bound microvesicles of endocytic origin. They are released into the extracellular environment after fusion with the plasma membrane (34, 36). Due to their purported role in intercellular communication, they can be readily taken up by cancer cells without the need for targeting ligands on the cancer cell surface (36). However, their reproducibility and cytotoxicity remain major concerns (24).

1.4.3 Cellular vehicles

Various cell types exhibiting tumor tropism have been considered as a potential vehicle for suicide gene therapy, including an endothelial progenitor precursor and stem cells such as mesenchymal stem cells (MSCs) (37) or neural stem cells (NSCs) (38). Employed cellular vehicles should be easy to isolate from different places inside the body and to transduce to express the suicide gene. MSCs are adult stem cells with an immunologic tolerance and an inherent migration ability. When engrafted, they preserve their tumor homing ability where they are involved in tumor stroma formation, making them a potential candidate to tackle current issues with viral vector usage (39).

1.5 Stem cells

Stem cells possess two important properties: they are capable of self-renewal where they undergo numerous cycles of cell division while maintaining their undifferentiated state and they can differentiate into a range of specialized cell types (40, 41). In adult organisms, stem cells repair the body where they replenish adult tissues but also maintain the normal turnover of regenerative organs such as the blood or skin.

Research has already employed bone marrow-derived mesenchymal stem cells (BM-MSCs) as a cellular vehicle. BM-MSCs are multipotent, stromal cells that can differentiate into osteoblasts, chondrocytes, myocytes and adipocytes (39, 42). They are autologously isolated from the bone marrow and then can be manipulated to express HSV1-sr39-tk. These HSV1sr39-tk-expressing BM-MSCs are then inserted back into the same patient, preventing an allogenic response to the carrier (25). However, bone marrow extraction is considered arduous for the patient (39, 42). Accordingly, other cellular vehicles with a less laborious extraction with the same characteristics as BM-MSCs can be very beneficial as a carrier: human dental pulp stem cells (hDPSCs; Figure 3).

1.5.1 Human dental pulp stem cells as a suicide gene carrier

Human DPSCs are a subtype of MSCs that have identical properties. They are nonhematopoietic, multipotent stem cells that are present in the dental pulp (43). Morphologically, they are fusiform with a central nucleus and a large cytoplasm. Human DPSCs are capable of self-renewal and are responsible for the maintenance and repair of tissue in the tooth (44). They are isolated by the enzymatic digestion method or the outgrowth method from third molars (45); third molars are considered waste material because they are removed for orthodontic reasons, making the isolation of hDPSCs less invasive than other stem cells such as BM-MSCs.

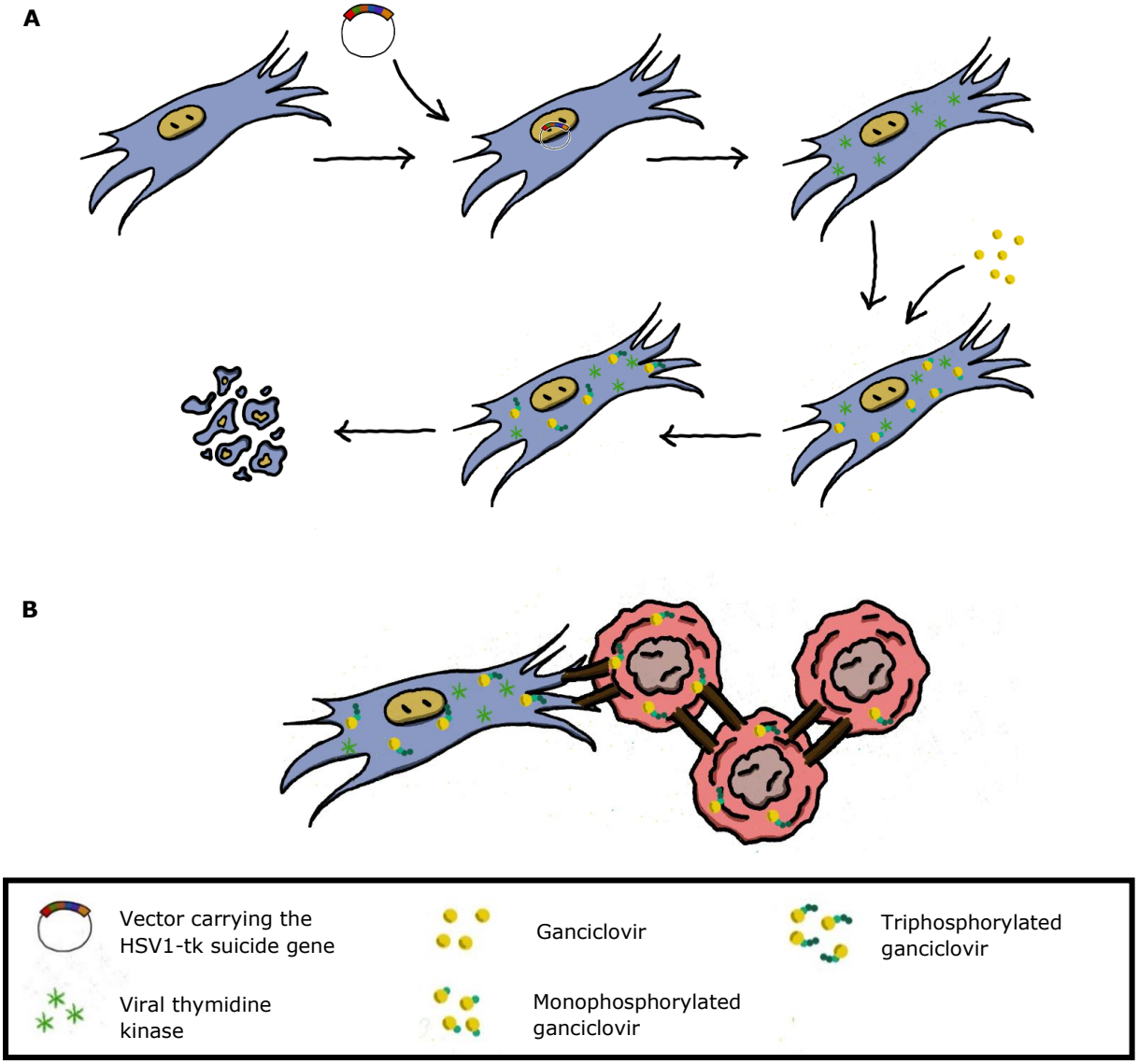

Figure 3 Overview HSV1-sr39-tk/GCV mechanism in hDPSCs and the bystander effect between hDPSCs and OSCC cells. A) *The viral vector containing the HSV1-sr39-tk suicide gene is inserted into the hDPSC. Upon uptake into the genome, the viral TK protein is expressed. The mechanism is identical to the cancer cell; however, the transduced hDPSCs are injected intratumorally and can form gap junctions with the cancer cells before the prodrug GCV is administered. Then, the viral TK monophosphorylates the GCV and further phosphorylation by endogenous cellular kinases leads to a triphosphorylated, toxic form of GCV (3P-GCV).* ***B)*** *This 3P-GCV migrates through the gap junctions into the cancer cells. 3P-GCV is incorporated into the cellular DNA leading to chain termination and apoptosis of both the hDPSC and connected cancer cells. This is the bystander effect. Abbreviations: TK, thymidine kinase; (3P-)GCV, (triphosphorylated) ganciclovir; hDPSCs, human dental pulp stem cells.*

Human DPSCs are characterized and identified by a panel of specific markers that are identical to MSC markers. These hDPSCs should be positive to cluster of differentiation (CD)29, CD44, CD59, CD73, CD90, CD105 and CD146 but should be negative for CD14, CD31, CD34, CD45 and HLA-DR (46). They should also adhere to plastic and require a fibroblast morphology. Human DPSCs can differentiate into chondrocytes, adipocytes, odontoblasts and neural-like cells under the appropriate induction conditions. For example, research indicated that in the process of differentiation of hDPSCs into odontoblasts similar biochemical pathways are implicated as involved in the differentiation of BM-MSCs into osteoblasts. Furthermore, hDPSCs have a higher proliferation rate, greater clonogenic potential and a higher number of progenitor cells in the population compared to BM-MSCs (47).

Human DPSCs have been shown to migrate towards tumor lesions due to chemokines such as stromal cell-derived factor-1 (SDF-1) or vascular endothelial growth factor (VEGF) that are expressed and released by the cancer cells (48-50). SDF-1 is a chemokine protein that has been observed in several malignancies (i.e., OSCC, melanoma) (51). OSCC cells highly express SDF-1 because the molecule is involved as a signaling molecule in OSCC cell invasion (52). Furthermore, SDF-1 has also been found during dental pulp inflammation (49) and the SDF-1/CXCR4 axis has been shown to play an essential role in mobilization, migration and homing in hDPSCs (53).

Human DPSCs are considered immuno-privileged as they are hypoimmunogenic. They are not direct immune effectors; however, they act indirectly in initiating an immune response by activating immune cells through signaling cascades such as nuclear factor kappa-light-chain-enhancer of activated B cells (NF-κB). NF-κB is a transcription factor that is important in the transcription of light chain κ immunoglobulin genes. It is present in almost all cells including hDPSCs (54). NF-κB plays a central role in immunity through the production and regulation of pro-inflammatory cytokines such as tumor necrosis factor (TNF)-α or interleukin (IL)-8. The expression of NF-κB in hDPSCs is related to the immunomodulatory properties of hDPSCs. Furthermore, depending on the activation of NF-κB the pro-inflammatory cytokine interferon-γ promotes the proliferation and migration of hDPSCs (44, 54).

Additionally, hDPSCs have also been reported to regulate the immune response in various diseases and therefore are considered immunomodulatory. Hereby, hDPSCs can modify the immune response by stimulating or suppressing it to maintain homeostasis. The underlying mechanism of the immunosuppressive properties of hDPSCs is the suppression of peripheral blood mononuclear cell proliferation through transforming growth factor (TGF) production (44, 55). Research has indicated that hDPSCs increase regulatory T cells and forkhead box P3 positive ($FOXP3^+$) *in vitro* because of production of TGF-β and IL-10 anti-inflammatory cytokines. This way, an immunotolerance is conferred to the hDPSCs (44).

These advantages make the hDPSCs an ideal candidate as a potential carrier for the HSV1-sr39-tk suicide gene. Therefore, we hypothesize that therapy with HSV1-sr39-tk-transduced hDPSCs results in the death of OSCC cells through the bystander effect (Figure 3B) and elicits a subsequent reduction in tumor size. When a hDPSC cell line that carries the HSV1-sr39-tk suicide gene is achieved and the HSV1-sr39-tk/GCV mechanism is optimized, these HSV1-sr39-tk^+ hDPSCs are evaluated in an *in vivo* model to assess their potential as a suicide gene carrier in therapy.

1.6 *In vivo* models to assess treatment for oral squamous cell carcinoma

New therapies can be investigated *in vivo* by using animal models that enable to study the complex biological process behind OSCC. In mouse models for OSCC, xenograft models and chemical carcinogen-induced models are extensively characterized (56). In xenograft models human OSCC cells are implanted into immunodeficient mice. They are frequently used to study tumor growth and its spreading but also to test and develop new potential drugs (56, 57). To investigate OSCC through carcinogen induction different models such as the dimethyl-1,2-benzanthracene model or the 4-nitroquinoline-1-oxide (4NQO) model have been used worldwide (56, 57).

The substance 4NQO is a derivative of tobacco and a water-soluble tumorigenic compound that induces DNA damage through the production of reactive oxygen species (ROS) (58). These effects are similar to the genetic and epigenetic alterations that result from tobacco exposure leading to the development of malignant lesions which resemble the morphology and histology of human OSCC (59). The 4NQO model is a multistep process in which invasive OSCC develops after six to ten months (Figure 4; (60)) (60, 61). The development of malignant OSCC is preceded by increasing grades of dysplastic changes (56). These tumors are used to study the therapeutic effect of various therapies including gene therapy (57, 62, 63).

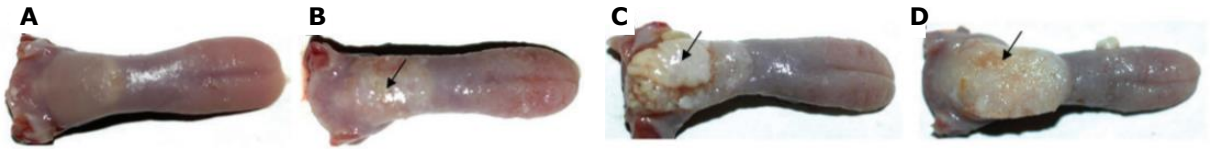

Figure 4 A rat model of oral carcinogenesis after ad libitum 4NQO administration through the drinking water. *Representative photographs of oral tumors developed in Sprague-dwaley rats:* ***A)*** *a propane diol-administered tongue (vehicle),* ***B)*** *after 80 – 120 days of 4NQO administration,* ***C)*** *after 160 days and* ***D)*** *after 200 days 4NQO administration through the drinking water. Arrows indicate tumor growth. Abbreviations: 4NQO, 4-nitroquinoline-1-oxide.*

1.6.1 Tumor analysis through magnetic resonance imaging

The use of magnetic resonance imaging (MRI) is an excellent way to examine structural changes such as tumor growth (64). MRI is a three-dimensional non-invasive imaging method that uses strong magnetic fields, magnetic field gradients and radio waves to generate images of organs in the body. When placed in a magnetic field, certain nuclei (e.g., hydrogen atoms) can absorb and emit radio frequency energy. The technique holds a high spatial resolution and is capable of morphological imaging (65).

However, when imaging mice image resolution can be a limiting factor (64). The size of their tongue and lesion size can pose issues in visualization. Therefore, opting for larger animal models (i.e., the rat) might address these limitations in administration and visualization. This potential new rat model for OSCC requires further characterization before potential treatment strategies can be investigated such as hDPSCs as a carrier for the HSV1-sr39-tk suicide gene to treat OSCC.

2 Materials and methods

2.1 pSINc-HSV1-sr39-tk-T2A-fLuc-IRES-PURO^R plasmid engineering

To engineer a plasmid that harbors both the HSV1-sr39-tk fragment and the firefly luciferase (fLuc) fragment and a control plasmid that contains an enhanced green fluorescent protein (eGFP) and fLuc fragment, inserts were ordered as sequenced GBlocks from Integrated DNA Technologies (IDT; Leuven, Belgium). The pSINc plasmid containing the elongation factor 1-α (EF1-α) promotor, the puromycin resistance cassette (PURO^R) and an ampicillin resistance gene was generated previously by the research group.

To have a working solution of the ordered HSV1-sr39-tk, fLuc and eGFP inserts the pBAD/TOPO® ThioFusion™ Expression kit (Invitrogen, Erembodegem, Belgium) was performed. Hereby, the insert was directly introduced into a plasmid vector and were digested with enzymes to start the ligation process.

The HSV1-sr39-tk-T2A fragment introduced in the TOPO® plasmid and the pSINc-internal ribosomal entry site (IRES)-PURO^R plasmid were restricted with PmeI and SbfI (New England BioLabs, Leiden, The Netherlands). The pSINc-IRES-PURO^R plasmid was dephosphorylated by shrimp alkaline phosphatase (rSAP; New England BioLabs) and both the plasmid and HSV1-sr39-tk-T2A fragment ran through a cycle of: thirty minutes on 37°C to allow restriction digestion, twenty minutes on 80°C to deactivate the restriction enzymes and were stored at 4°C until further use.

The restricted fragments were isolated via agarose gel electrophoresis (Supplemental methods, 6.1.1 agarose gel electrophoresis) and the desired fragments were cut out of the agarose gel followed by gel extraction with the NucleoSpin® Gel and PCR clean-up kit (Macherey-Nagel, Eupen, Belgium). The HSV1-sr39-tk-T2A fragment and pSINc-IRES-PURO^R plasmid were ligated (ratio 3:1, respectively) using the T4 ligase enzyme (New England BioLabs) for two hours on 22°C followed by an inactivation step of ten minutes on 65°C and the ligation product was stored on 4°C until further use. Transformation of 5 µL ligation product was performed employing 25 µL chemically competent *E. coli* (NEB® 5-alpha competent, New England BioLabs) which could grow overnight (37°C) on ampicillin-enriched agar plates (50 mg/mL ampicillin; Invitrogen). Colonies were picked and transferred to new agar plates as a back-up for potential HSV1-sr39-tk-harboring colonies while the pipette tip used to pick the colonies was incubated shaking (200 rotations per minute [rpm]) overnight (37°C) in 1.5 mL ampicillin-enriched LB Broth (50 mg/mL ampicillin; Invitrogen) to allow expansion of colonies that have taken up the ligated plasmid.

The following day, the Nucleospin® Plasmid EasyPure (Macherey-Nagel) extraction kit was employed to extract high-purity plasmid DNA from LB broth-grown colonies. A restriction pattern was created through restriction digestion with KspaI and NheI (Thermofisher Scientific, Erembodegem, Belgium) or BamHI (New England BioLabs) followed by agarose gel electrophoresis. Successfully engineered plasmids (Figure 5) were selected and their DNA concentration was determined through Nanodrop® (Thermofisher Scientific).

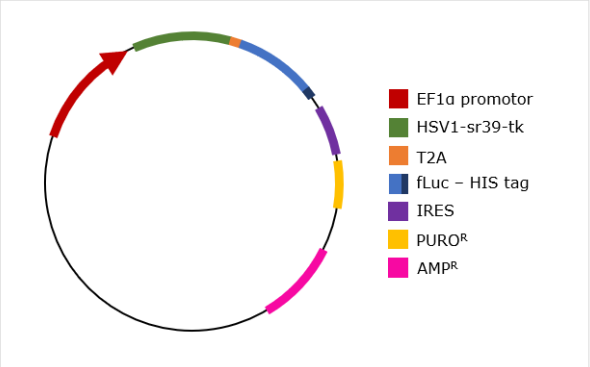

Figure 5 The pSINc-HSV1-sr39-tk-T2A-fLuc-IRES-PURO^R plasmid requires insertion of HSV1-sr39-tk and fLuc. *Abbreviations: EF1-α, eukaryotic translation elongation factor 1-alpha promotor; HSV1-sr39-tk: herpes simplex virus 1-sr39-thymidine kinase gene; T2A: self-cleaving 2A peptide, variant T; fLuc: firefly luciferase; IRES: internal ribosomal entry site; PURO^R: puromycin resistance gene*

Next, the fLuc fragment and the pSINc-HSV1-sr39-tk-T2A-IRES-PURO^R plasmid were digested using MreI and KspaI (Thermo Scientific) and the fLuc fragment was introduced into the plasmid with KspAI and MreI in an identical procedure as the HSV1-SR39-tk-T2A fragment. The restriction pattern of the plasmid was determined using NdeI and HpaI or BamHI (New England BioLabs).

The control plasmid containing no HSV1-sr39-tk-T2A fragment but an eGFP-T2A fragment was prepared by digesting the HSV1-sr39-tk-T2A fragment out of the finished plasmid with NheI and MreI (Thermofisher Scientific) and introducing the eGFP-T2A fragment. The restriction pattern after ligation was determined through a restriction digestion with BamHI (New England BioLabs).

2.2 Cell cultures

2.2.1 Cell culturing of human dental pulp stem cells

Human DPSCs were isolated from third molars which were removed for orthodontic reasons. Prior to isolation, patients gave their informed consent (B371201419770/A/U). Isolation of hDPSCs was executed through the outgrowth method as described by Hilkens et al. (45). Cells were cultured (37°C, 5% CO_2) on alpha-modified minimum essential medium (α-MEM; Sigma-Aldrich, Overijse, Belgium) supplemented with 2 mM L-glutamine (Sigma-Aldrich), 100 U/mL penicillin (Sigma-Aldrich), 100 µg/mL streptomycin (Sigma-Aldrich) and 10% fetal bovine serum (FBS; BioWest, Nuaille, France). Cell culture medium was refreshed every two to three days. Cells were subcultured weekly using trypsin-EDTA (Gibco Life Technologies, Merelbeke, Belgium) when 70 – 80% confluency was reached.

2.2.2 Cell culturing of University of Michigan-Squamous cell carcinoma-14C cells

University of Michigan-Squamous cell carcinoma-14C cells (UM-SCC-14Cs; CLS Cell Lines Service, Eppelheim, Germany), further named OSCC cells during this project, were cultured (37°C, 5% CO_2) in Dulbecco's Modified Eagle Medium (DMEM; nutrient mix F12, Sigma-Aldrich) supplemented with 2 mM L-glutamine, 100 U/mL penicillin, 100 µg/mL streptomycin and 5% FBS. Cell culture medium was refreshed every two to three days and cells were subcultured at 70 – 80% confluency using Accutase® (Innovative Cell Technologies Inc., San Diego, United States).

2.2.3 Co-culture of human dental pulp stem cells and University of Michigan-Squamous cell carcinoma-14C cells

For the co-culture staining experiments, UM-SCC-14Cs and hDPSCs were cultured (37°C, 5% CO2) in 24-well plates (Greiner Bio-One, Vilvoorde, Belgium) in DMEM/F12 supplemented with 5% FBS, on glass coverslips at a density of $1x10^4$ cells per well (ratio of 1:1, hDPSC:UM-SCC-14C). For the connexin-43 (Cx-43) staining, cells were left to rest for at least two days to allow gap junction formation after reaching confluency.

For the Lucifer Yellow experiment, UM-SCC-14Cs and hDPSCs were cultured (37°C, 5% CO2) in 35 mm #1.5 glass dishes (P35G-1.5-20-C; MatTek, Istanbul, Turkey) in DMEM/F12 supplemented with 2 mM L-glutamine, 100 U/mL penicillin, 100 µg/mL streptomycin and 5% FBS at a density of $20x10^4$ cells per dish (ratio of 1:1, hDPSC:UM-SCC-14C). They were then left to rest for at least two days to allow gap junction formation between cells prior to the start of the experiment.

2.3 Assessing gap junction presence through a connexin-43 staining

Co-cultures seeded to full confluency (hDPSC:OSCC, 1:1 ratio) in 24-well plates were left to allow gap junction formation for at least two days. Next, cells were fixed by Unifix® (Klinipath, Duiven, The Netherlands) for twenty minutes at room temperature. Subsequently, cells were washed thrice with phosphate buffered saline (PBS; Lonza, Bazel, Switzerland) and before staining, the glass coverslips containing the co-culture were transferred to a new well plate. Coverslips were incubated for thirty minutes with 10% protein block (Ready-to-use, Dako, Erembodegem, Belgium) followed by exposure to the primary anti-Cx-43 antibody (0.8 µg/mL; ab11370, Abcam, Leuven, Belgium) overnight at 4°C. Next, the co-culture was exposed to the secondary antibody (Goat anti-Rabbit IgG-HRP, Dako) which was incubated at room temperature in the dark for thirty minutes. A DAB (3,3-diaminobenzidine, Dako) staining was performed until a brown staining was visible (or eight minutes maximum) followed by a nuclear counterstain with Mayer's hematoxylin (Leica, Amsterdam, The Netherlands) for five minutes. Between each step, coverslips were washed in PBS. Lastly, glass coverslips were mounted using Immu-Mount™ (Thermofisher Scientific) and they were left to dry overnight at room temperature. Coverslips were analyzed by a brightfield light microscope (Leica Face-to-Face, DM2000).

2.4 Visualizing human dental pulp stem cells and University of Michigan-Squamous cell carcinoma-14c cells through surface markers

Individual hDPSCs or individual OSCC cells were grown on glass coverslips to 70 – 80% confluency in a 24-well plate before fixation with Unifix® for twenty minutes at room temperature. Prior to the staining procedure, cells were washed thrice with PBS and the coverslips were transferred to a new 24-well plate. Next, coverslips were incubated with 10% protein block for thirty minutes prior to primary antibody incubation (Table 1) for one hour at room temperature. Following day, the cells are exposed to the secondary antibody (Goat anti-Rabbit/Mouse IgG-HRP) and incubated at room temperature in the dark for thirty minutes. A DAB staining was performed until a brown staining was visible (or eight minutes maximum) followed by a counterstain with Mayer's hematoxylin for five minutes. Between each step, glass coverslips were rinsed with PBS. The coverslips were mounted

with Immu-mount™ and left overnight to dry at room temperature. Coverslips were analyzed with a brightfield light microscope (Leica Face-to-Face, DM2000, Wetzlar, Germany).

Human DPSCs and OSCC cells were grown on glass coverslips in a co-culture (1:1 ratio, hDPSC:OSCC) to 70 – 80% confluency in a 24-well plate. The same protocol was followed to visualize the co-culture; however, either the antibody against CD90 (hDPSC) or EpCAM (OSCC) were incubated for one hour at room temperature or the primary antibodies were incubated together for one hour at room temperature for a double immunofluorescence staining. Next, secondary antibodies Goat anti-Mouse 555 (against CD90; Life Technologies, Belgium) or/and Goat anti-Rabbit 647 (against EpCAM; Life Technologies) were incubated for thirty minutes in the dark at room temperature. Cells were counterstained with 4',6-diamidino-2-fenylindool (DAPI; 1:25, Dako) for 10 minutes at room temperature and mounted with Immu-mount™ (Thermofisher Scientific) prior to visualization with a fluorescence microscope (Leica DM 4000 BLED, Wetzlar, Germany). For the live staining, the antibody against CD90 was incubated overnight at 37°C before incubation with the secondary antibody Goat anti-Mouse 555 for thirty minutes in the dark at room temperature. Cells were rinsed with PBS and replenished with standard OSCC growth medium prior to the dye coupling experiment.

Table 1 Employed antibodies to discern human dental pulp stem cells from oral squamous cell carcinoma cells

Primary Antibody	End dilution, Company	Secondary antibody	Cell staining
CD73	1:50, Biolegend, San Diego, United States	Goat anti-Mouse IgG-HRP (Dako)	hDPSC
CD90	1:50 on fixed cultured cells; 1:100 on co-culture (live) cells, Biolegend	Goat anti-Mouse IgG-HRP (Dako) Goat anti-Mouse 555 (Life Technologies, A21422)	hDPSC
EpCAM	1:400, Abcam (ab71916)	Goat anti-Rabbit IgG-HRP (Dako) Goat anti-Rabbit 647 (Life Technologies, A2A247)	OSCC
Laminin	1:100, Abcam (ab7463)	Goat anti-Rabbit IgG-HRP (Dako)	OSCC

2.5 Assessing gap junction functionality by live-imaging through micro-injection with Lucifer Yellow

For a pilot experiment to assess the potential of visualizing dye coupling, hDPSCs were seeded to full confluency on 35 mm #1.5 glass dishes (P35G-1.5-20-C) and left to rest for two days to allow gap junction formation. Cells were replenished with standard OSCC growth medium every two days until start of the experiment. Gap junction functionality was assessed by loading one single hDPSC with Lucifer Yellow (Sigma-Aldrich) through micro-injection. The growth medium of the hDPSCs was replaced with a bath solution containing 145 mM NaCl, 1.5 mM KCl, 2 mM $CaCl_2$, 2 mM $MgCl_2$, 10 mM HEPES and 10 mM glucose, adjusted to pH 7.4 (Sigma-Aldrich). Micropipettes (2-5 MΩ resistance) were fabricated from 1.5 mm (o.d.) borosilicate glass capillary tubes. The pipette working solution contained 1 mg/mL Lucifer Yellow in 125 mM KCl, 1 mM $CaCl_2$, 2 mM $MgCl_2$, 2 mM Mg-ATP, 2 mM Na_2ATP, 10 mM HEPES, 10 mM EGTA, adjusted to pH 7.2 (Sigma-Aldrich) and was

iontophoretically injected into the hDPSCs. Immediately after injection and during the crossing of Lucifer Yellow through the gap junctions (approximately five to ten minutes) the dye was visualized using an inverted laser-scanning microscope (Zeiss Elyra PS.1, Cologne, Germany) and a 63x/1.4 oil immersion objective emitting at 405 nm with a band-pass filter of 495 – 575 nm to filter emission light.

Next, dye coupling was observed in a co-culture of hDPSCs and OSCC cells (ratio 1:1, hDPSC:OSCC). Cells were seeded to full confluency in 35 mm #1.5 glass dishes and left to rest for an additional two days to allow gap junction formation. Cells were replenished with OSCC growth medium every two days until start of the experiment. Cells were stained with CD90 as previously described. hDPSCs were visualized by emitting at 488 nm with a bandpass filter of 570 – 650 nm and a longpass filter of 750 nm. Following, dye coupling by micro-injection of Lucifer Yellow was performed as previously described.

2.6 Assessing tumor growth in the 4-nitroquinoline-1-oxide rat model

Wistar rats were exposed to 4NQO (201424V1, UHasselt; Sigma-Aldrich) through two different routes: either the substance was administered through the drinking water at libitum (n = 27; 0.01 mg/mL) or the animals were anesthetized, and the substance was topically applied onto the tongue (n = 27; 5 mg/mL dissolved in propylene glycol – 3 times per week). Three animals per administration route were euthanized each month. Their tongues were extracted, scanned using *ex vivo* MRI and histological slices were assessed for tumor growth. Control animals were also divided into two groups: either they were anesthetized and propylene glycol (vehicle) was applied onto the tongue (n = 3) or animals did not undergo any procedures (n = 3). All control animals were euthanized at the end of the experiment and underwent identical procedures as experimental animals.

2.6.1 Histochemical analysis via a Masson's trichrome staining

Rat tongue sections were deparaffinized (twice in xylene [Sigma Aldrich] followed by twice in ethanol 100%, ethanol 95%, ethanol 80%, ethanol 70% [VWR, Oud-Heverlee, Belgium] and distilled water for two minutes per solution). Masson's trichrome staining was performed as follows: nuclei were stained employing Mayer's hematoxylin for five minutes. Afterwards, sections were rinsed in water for a minimum of thirty minutes and a Ponceau/Fuchsine stain (Sigma-Aldrich) was executed for five minutes to visualize collagen in the sample. Following, sections were exposed for five minutes to phosphomolybdic acid (1%, Sigma-Aldrich). Aniline Blue (Sigma-Aldrich) was employed for eight minutes to visualize the connective tissue. Between each staining solution slices were rinsed in distilled water for two minutes. Another phosphomolybdic acid (1%) staining was performed before sections were rinsed in distilled water for thirty seconds followed by acetic acid (1%; Merck, Overijse, Belgium) to produce a more delicate shade of tissue coloration. Rat tongue sections were then dehydrated (ethanol 70%, ethanol 80%, ethanol 95%, twice in ethanol 100% and twice in xylene for two minutes per solution). Furthermore, slices were mounted by using DPX (Merck) and analyzed by a panoramic viewer (3D Histech Confocal, Sysmex, The Netherlands) and the CaseViewer™ software.

2.6.2 Immunohistochemical analysis

Rat tongue sections were first deparaffinized thrice in xylene, followed by thrice in ethanol 100%, once in ethanol 70% and distilled water for two minutes per solution. Next, antigen retrieval was performed in citrate buffer (pH 6.0; Merck) that was heated, and sections were allowed to rest for thirty minutes. For the anti-p53 primary antibody heavy antigen retrieval was performed (Supplemental methods, 6.1.2 Heavy antigen retrieval). Sections were lined with a PAP pen (Dako) before peroxidase blocking (Invitrogen) for twenty minutes. Next, a 10% protein blocking was done for thirty minutes before introducing the primary antibody (Table 2) in 10% protein block and left on 4°C overnight. Between each step, sections were washed thrice in PBS for five minutes.

The following day, sections were washed five times with PBS for five minutes before introducing the secondary antibody (Table 2) that was incubated on room temperature for thirty minutes in the dark and then washed with PBS. Next, a DAB staining was performed until a brown staining was visible (or for eight minutes maximum) followed by a nuclear counterstaining with Mayer's hematoxylin for five minutes. Sections were then washed with tap water for five minutes followed by dehydration (ethanol 70%, thrice in ethanol 100% and thrice in xylene for two minutes per solution). Lastly, slides were mounted with DPX. Slides were analyzed by a panoramic viewer (3D Histech Confocal, Sysmex, The Netherlands) and the CaseViewer™ software.

Table 2 Employed primary antibodies, their concentration, and their respective secondary antibodies.

Primary Antibody	End dilution, Company	Information	Secondary antibody
Anti-p63	1:200, Abcam	Rabbit monoclonal (ab124762)	Goat Anti-Rabbit HRP (Dako)
Anti-p53	1:100, Invitrogen	Mouse monoclonal (ab-2533019)	Goat Anti-Mouse HRP (Dako)
Anti-CD44	1:1000, Abcam	Rabbit polyclonal (ab157107)	Goat Anti-Rabbit HRP
Anti-Ki67	1:500, Abcam	Rabbit polyclonal (ab15580)	Goat Anti-Rabbit HRP
EGFR	1:25, ThermoFisher	Mouse monoclonal (MA5-13070)	Goat Anti-Mouse HRP
MAGEA-3	1:50, Merck	Rabbit polyclonal (ABC468)	Goat-Anti-Rabbit HRP
MAGEA-4	1:200, ThermoFisher	Rabbit polyclonal (PA5-72867)	Goat Anti-Rabbit HRP

3 Results

3.1 pSINc-HSV1-sr39-tk-T2A-fLuc-IRES-PURO^R plasmid engineering

A plasmid encoding the suicide gene and an imaging reporter gene was constructed. Two pSINc plasmid variants (A and C) were employed; these variants are different elutions of the same generated starting plasmid. Restriction digestion of the pSINc-IRES-PURO^R plasmid (Figure 6, lane two and three) and the HSV1-sr39-tk-T2A GBlocks fragment (Figure 6, lane four) with PmeI and SbfI shows distinct fragments around ± 7.5kb for the digested plasmid and ± 1.2kb for the HSV1-sr39-tk-T2A fragment when analyzed via agarose gel electrophoresis. These fragments are isolated, purified and ligated.

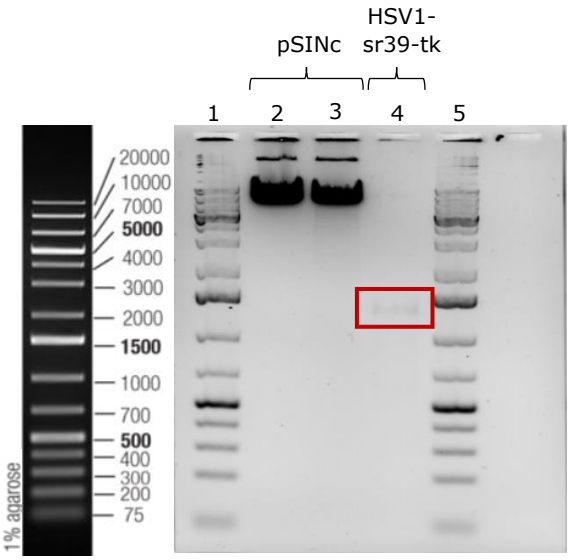

Figure 6 Agarose gel electrophoresis of the digested pSINc-IRES-PURO^R plasmid and the HSV1-sr39-tk-T2A fragment shows distinct fragments near 7.5kb for the plasmid variants and 1.2kb of the HSV1-sr39-tk fragment. *Lane one and five depict the 1kb Plus ladder. The A and C variants of the pSINc-IRES-PURO^R plasmid fragments are shown in lane two and three at approximately 7.5kb. The fragment of HSV1-sr39-tk-T2A (red box, lane four) is present near approximately 1.2kb.*

After ligation of the pSINc-IRES-PURO^R plasmid and the HSV1-sr39-tk-T2A fragment, a transformation in NEB-α *E. coli* leads to the formation of colonies (Figure 7). The pSINc A variant shows increased colony formation compared to the negative control (only the vector was added) although the pSINc C variant shows little colony formation.

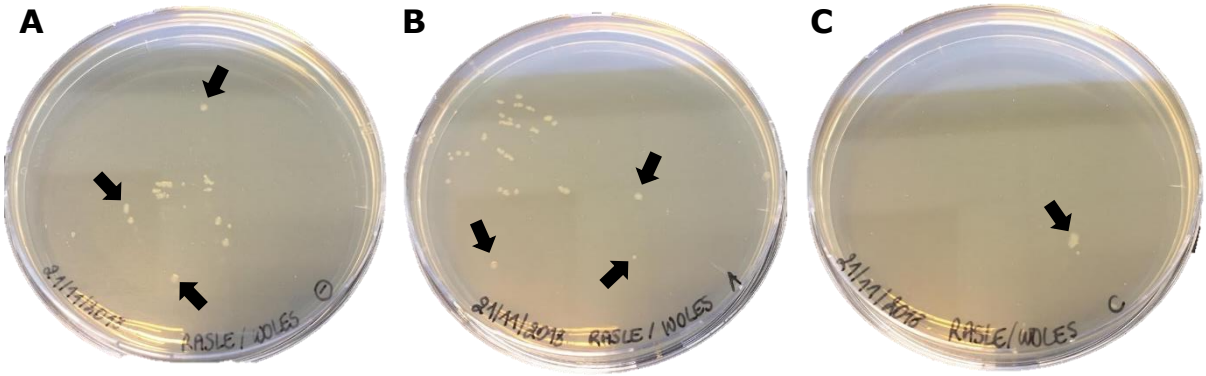

Figure 7 Colony formation after ligation of the pSINc-IRES-PURO^R vector and the HSV1-sr39-tk fragment. A) *The negative control was not ligated with the HSV1-sr39-tk-T2A fragment and shows moderate colony formation,* ***B)*** *the pSINc A variant ligated with the HSV1-sr39-tk-T2A fragment shows increased colony formation compared to the negative control and* ***C)*** *the pSINc C variant ligated with the HSV1-sr39-tk-T2A fragment shows little colony formation. Colony formation is indicated through black arrows.*

Plasmid DNA is extracted from picked colonies and a restriction pattern is created with KspAI and NheI to determine HSV1-sr39-tk-T2A presence in the plasmid. Analysis via agarose gel electrophoresis shows a distinct fragmentation at 1.2kb for three samples (Figure 8 lane 6 [pSINc A s5], lane 7 [pSINc A s6] and lane 12 [pSINc A s11]). Lane 13 is a potentially ligated HSV1-sr39-tk plasmid transformed with NEB-α *E.coli* that had been stored at -20°C. Commonly, these bacteria are usually stored on -80°C for an optimal transformation process.

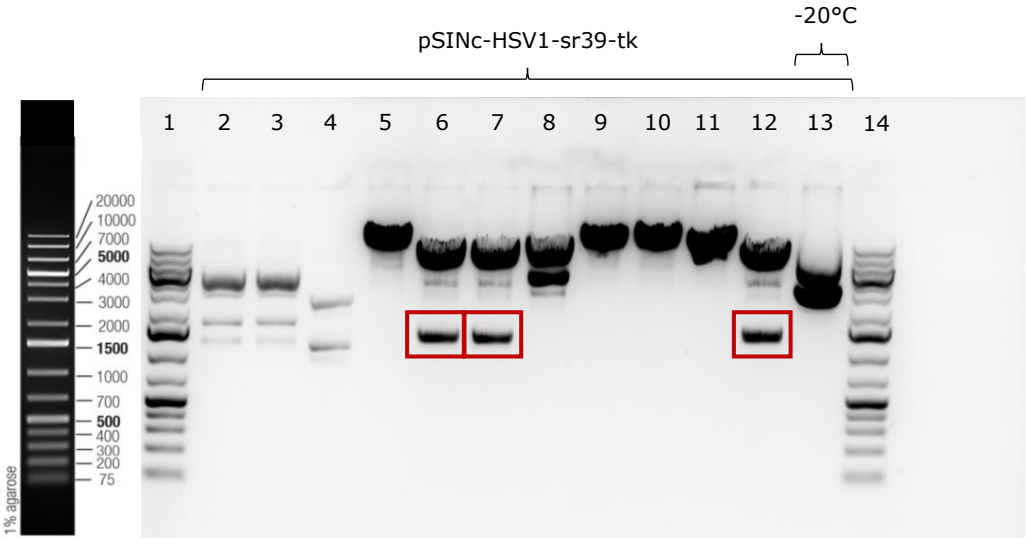

Figure 8 Restriction pattern shows successive transformation of three samples of the HSV1-sr39-tk-T2A fragment and the pSINc A-EF1-α-IRES-PURO^R plasmid. *Lane 1 and 14 depict the 1kb Plus ladder and lane 2 up until 13 depict different colony samples (s) of picked colonies. Colony samples in lane 6, 7 and 12 (pSINc A s5, pSINc A s6 and pSINc A s11, respectively) show the expected fragment (red boxes) near 1.2kb. Lane 13 (pSINc A s12) was ligated with NEB-α E.coli stored on -20°C instead of the commonly stored -80°C.*

Next, the fLuc fragment is introduced into the HSV1-sr39-tk-containing plasmid. Restriction digestion of the pSINc-HSV1-sr39-tk-T2A-IRES-PURO^R plasmid and the fLuc fragment by MreI and KspAI depicts distinct fragments at approximately 8kb (Figure 9 lane two and three) and 1.7kb (Figure 9 lane four) respectively after agarose gel electrophoresis.

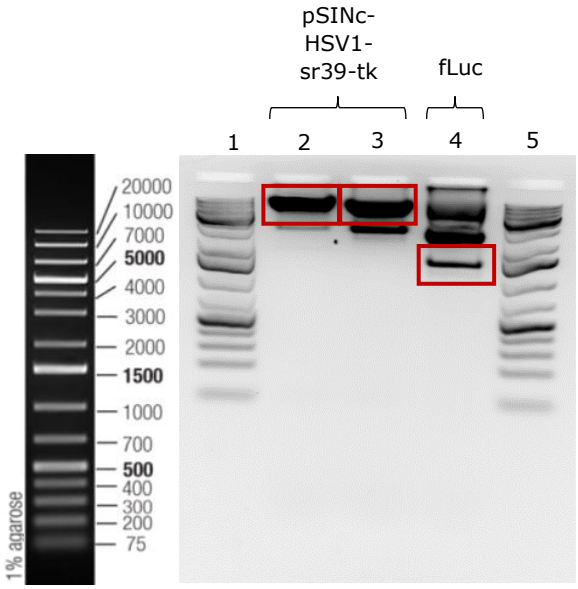

Figure 9 Agarose gel electrophoresis of the digested pSINcA-HSV1-sr39-tk-T2A-IRES-PURO^R plasmid and the fLuc fragment shows distinct fragments near 8kb for the plasmids and 1.7kb of the fLuc fragment. *Lane one and five depict the 1kb Plus ladder, while lane two and three depict the plasmid and lane four depicts the fLuc fragment. Lane two and three shows distinct fragmentation around 8kb (red box), and lane four shows a fragment approximately at 1.7kb (red box).*

Ligation of the pSINc-HSV1-sr39-tk-T2A-IRES-PURO^R plasmid and the fLuc fragment shows limited growth in the negative control plate (only the vector was added, Figure 10A). However, considerate colony formation is depicted on the plates where the fLuc fragment was inserted into the reaction, employing two different HSV1-sr39-tk-T2A plasmid samples (s5 and S6, Figure 10B-C, respectively).

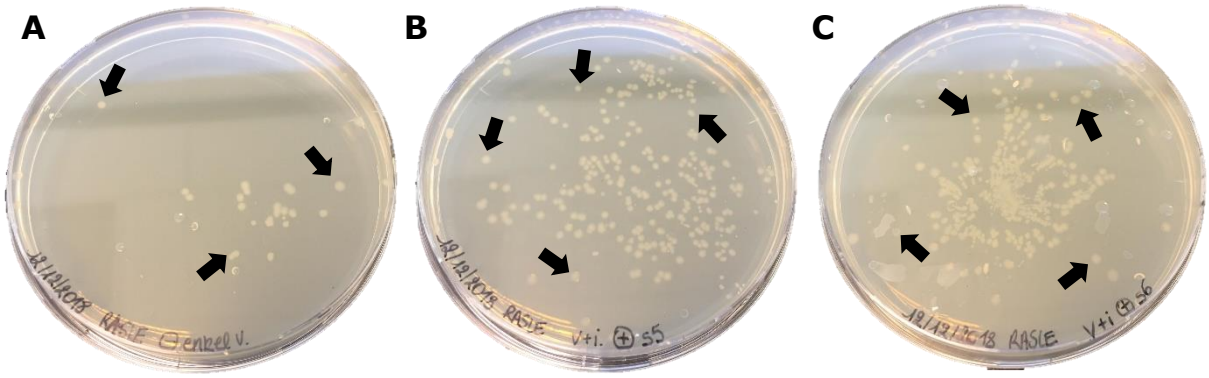

Figure 10 Colony formation after ligation of the pSINc-HSV1-sr39-tk-T2A-IRES-PURO^R vector and the fLuc fragment. A) *The negative control where no insert DNA was added to the ligation reaction shows little colony formation,* ***B)*** *The pSINc A s5 and* ***C)*** *the pSINc A s6 variant which hold the HSV1-sr39-tk fragment show considerable colony formation (black arrows).*

A restriction pattern is created for the extracted plasmid DNA with or HpaI and NdeI or BamHI assuring the presence of the fLuc fragment in the pSINc-HSV1-sr39-tk-T2A-IRES-PURO^R plasmid. Analysis of the electropherogram shows fragmentation at the expected 1.7kb for eight samples (Figure 11 lane four [pSINc A s6F3], lane five [pSINc A s6F4] and lane eight to thirteen [pSINc A s6F7 to s6F12, respectively]).

Furthermore, a negative control plasmid is generated encoding the eGFP gene instead of the HSV1-sr39-tk suicide gene, enabling a fluorescent signal in the transduced hDPSCs. The HSV1-sr39-tk gene is digested out of the plasmid by NheI and MreI and eGFP is introduced in the same restriction sites. The presence of eGFP is determined by BamHI restriction digestion. However, in the completed eGFP plasmid an unexpected additional fragment is observed.

Therefore, the insertion of the HSV1-sr39-tk gene was restarted into the EF1-α-IRES-PURO^R plasmid. After a restriction digestion with SbfI and PmeI followed by its respective ligation and plasmid purification, similar fragmentation patterns are seen (data not shown): one fragment near 1.2kb (expected fragment for HSV1-sr39-tk), one fragment near 8 – 9kb (the expected fragment for the plasmid without HSV1-sr39-tk), and one additional fragment near 2.8 – 3kb. Another experiment, where both the ordered HSV1-sr39-tk-T2A insert are tested and the insert introduced into the TOPO vector is digested with or without rSAP. Results indicate the presence of the same additional 2.8 – 3kb fragment (data not shown), along with the expected fragmentation pattern.

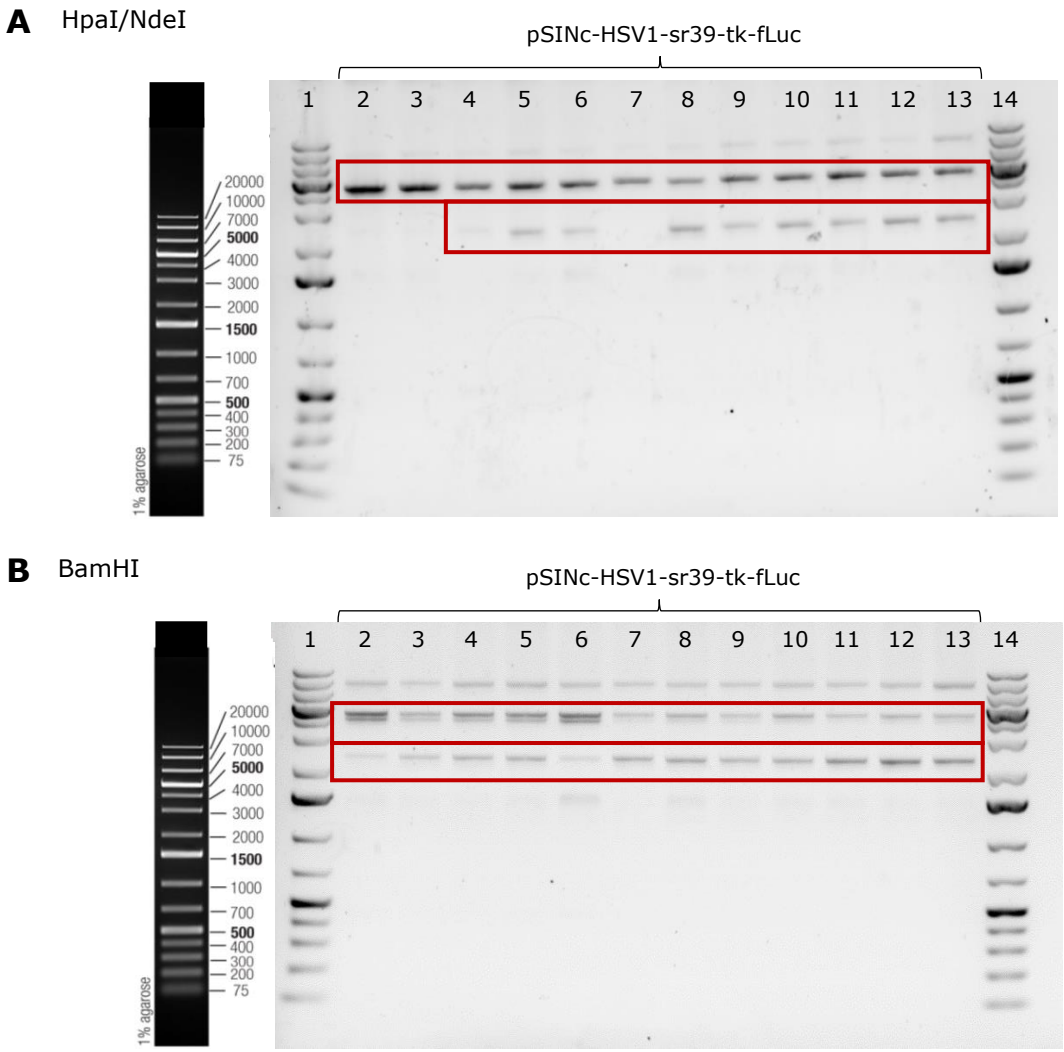

Figure 11 Restriction pattern showing successive transformation of eight samples of the pSINc A-HSV-tk-T2A-IRES-PURO^R plasmid and the Fluc fragment. *Lane one and fourteen depict the 1kb Plus ladder, while lane two up until thirteen depict different samples (s6F) of picked colonies digested with* ***A)*** *NdeI and HpaI or* ***B)*** *BamHI. Eight samples (s6F3, s6F4 and s6F7 to s6F12) show the expected fragmentation (red boxes) near 1.7kb and 8.8kb.*

3.2 Gap junction presence evaluation through connexin-43 immunocytochemistry

To ascertain gap junction formation, co-cultures of hDPSCs and OSCC cells are stained with an antibody against Cx-43 (Figure 12). Connexin-43 presence can be observed where brown staining is visible (red arrows). The DAB staining can be observed on both cell types but is more prominent in cell-dense regions. Black arrows indicate connections between OSCC cells.

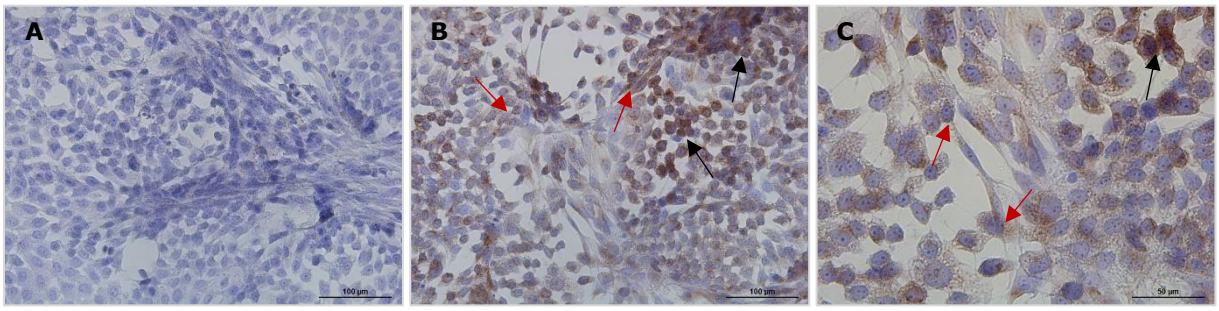

Figure 12 Connexin-43 staining in a co-culture of hDPSCs and OSCC cells indicates gap junction presence. A) *A negative control where no primary antibody was added shows no DAB staining in the sample (scale bar 100 µm).* ***B)*** *A co-culture of hDPSCs and OSCC cells indicates Cx-43 presence between cells. A more intense staining is observed in cell-dense regions (scale bar 100 µm) and* ***C)*** *the enlarged image of these cell dense regions emphasizes Cx-43 expression between hDPSC and OSCC cells (scale bar 50 µm). Red arrows: Cx-43 expression between hDPSCs and OSCC cells; black arrows: Cx-43 expression between OSCC cells. Abbreviations: Cx-43, connexin-43; hDPSCs, human dental pulp stem cells; OSCC, oral squamous cell carcinoma.*

3.3 Distinction of hDPSCs and OSCC cells through immunocytochemical staining

To discern hDPSCs and OSCC cells from one another in a co-culture various immunocytochemical markers are analyzed. These markers are selected according to the literature; they should be positive for either OSCC cells or hDPSCs while granting a negative staining in the other cell culture. Figure 13 indicates an intense DAB staining for endothelial cell adhesion molecule (EpCAM) and laminin in OSCC cells; however, this staining cannot be observed in hDPSCs. The two markers CD73 and CD90 are intensely stained in hDPSCs but staining is absent in OSCC cells.

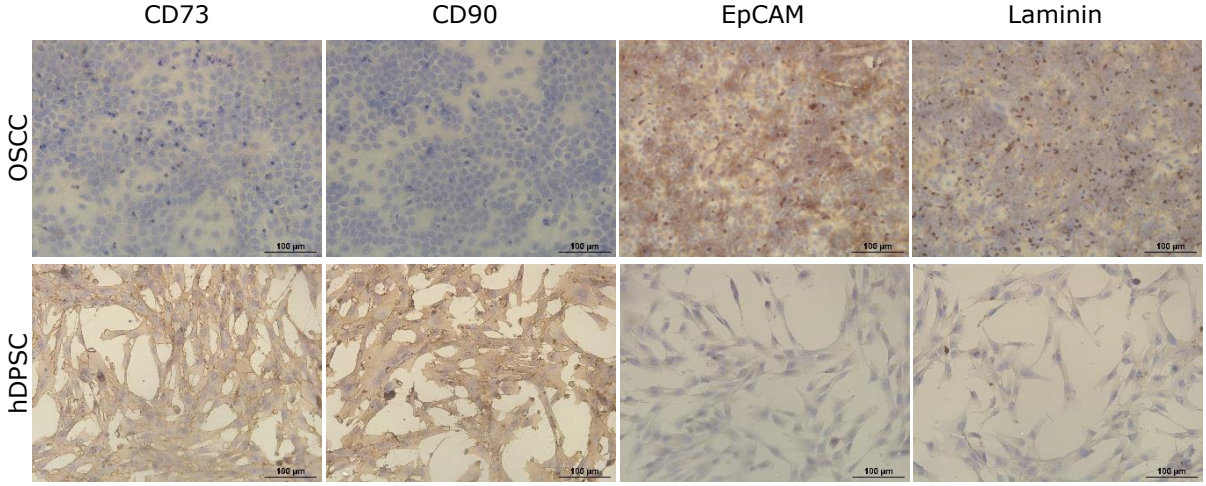

Figure 13 Immunocytochemical analysis indicates possibility of distinction between hDPSCs and OSCC cells. *CD73 and CD90 are negative (not stained) in an OSCC cell culture; however, an intense brown staining is observed in a hDPSC cell culture. Additionally, antibodies against EpCAM and laminin show an intense staining in the OSCC cell culture, but not in the hDPSC cell culture. Scale bars 100 µm. Abbreviations: EpCAM, Epithelial Cell Adhesion Molecule; OSCC, oral squamous cell carcinoma cells; hDPSC, human dental pulp stem cells.*

Next, the markers for CD90 and EpCAM are selected for fluorescent visualization. Co-cultures are stained either with an antibody against CD90 or against EpCAM (Figure 14A-B, respectively). Either hDPSC (Figure 14A) or OSCC cells (Figure 14B) can be distinguished in a fluorescent staining against their respective antibodies. A fluorescent double staining of CD90 and EpCAM to discern hDPSCs from OSCC cells is depicted in Figure 14D. EpCAM is shown in green, while CD90 is shown in red. OSCC cells and hDPSCs are interlaced and visually discerned through their respective fluorescent color. Nuclei are counterstained with a DAPI staining.

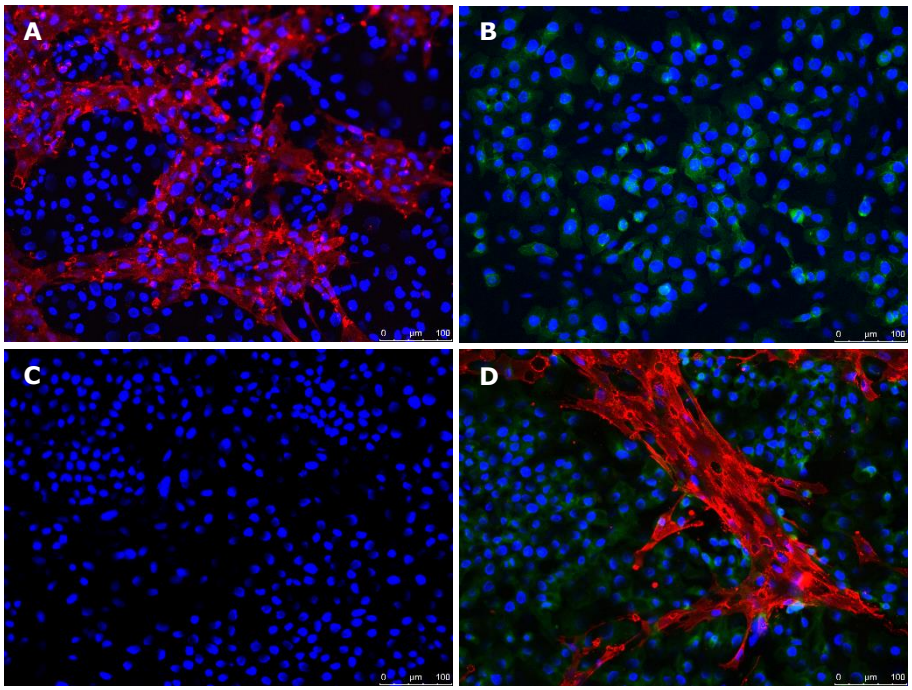

Figure 14 Markers CD90 and EpCAM specifically visualize hDPSCs and OSCC cells respectively. *In a co-culture, cells were stained with antibodies against:* ***A)*** *CD90 (1:50),* ***B)*** *EpCAM (1:400),* ***C)*** *no antibody (negative control) except a nuclear DAPI staining and* ***D)*** *CD90 and EpCAM in a double staining. Cells can be discerned through their nuclei stained with DAPI (blue) where OSCC cells have a large, round nucleus while hDPSCs have a more oval-shaped, smaller nucleus. CD90 is indicated in red, EpCAM is indicated in green. Scale bars: 100 µm. Abbreviations: DAPI, 4',6-diamidino-2-phenylindole; EpCAM, epithelial cell adhesion molecule; hDPSCs, human dental pulp stem cells; OSCC, oral squamous cell carcinoma.*

3.4 Gap junction functionality assessment through live-imaging via micro-injection with Lucifer Yellow

In a pilot experiment, hDPSCs are seeded to full confluency and allowed to rest for two days to allow gap junction formation. Next, a singular hDPSC is injected with the fluorescent dye Lucifer Yellow, allowing the distinction of this cell from others through the fluorescent signal (Figure 15A; 0 min). As time progresses, the fluorescent dye flows from the primarily injected hDPSC and spreads to surrounding cells (Figure 15A; 4 – 8 min). When the fluorescent channel is overlain with its respective brightfield image, this fluorescent signal can be detected where hDPSCs are present while no fluorescent signal is detected outside the respective hDPSCs. An overview image with the micro-injected hDPSC in the center shows a network of fluorescent signal in surrounding hDPSCs (Figure 15B).

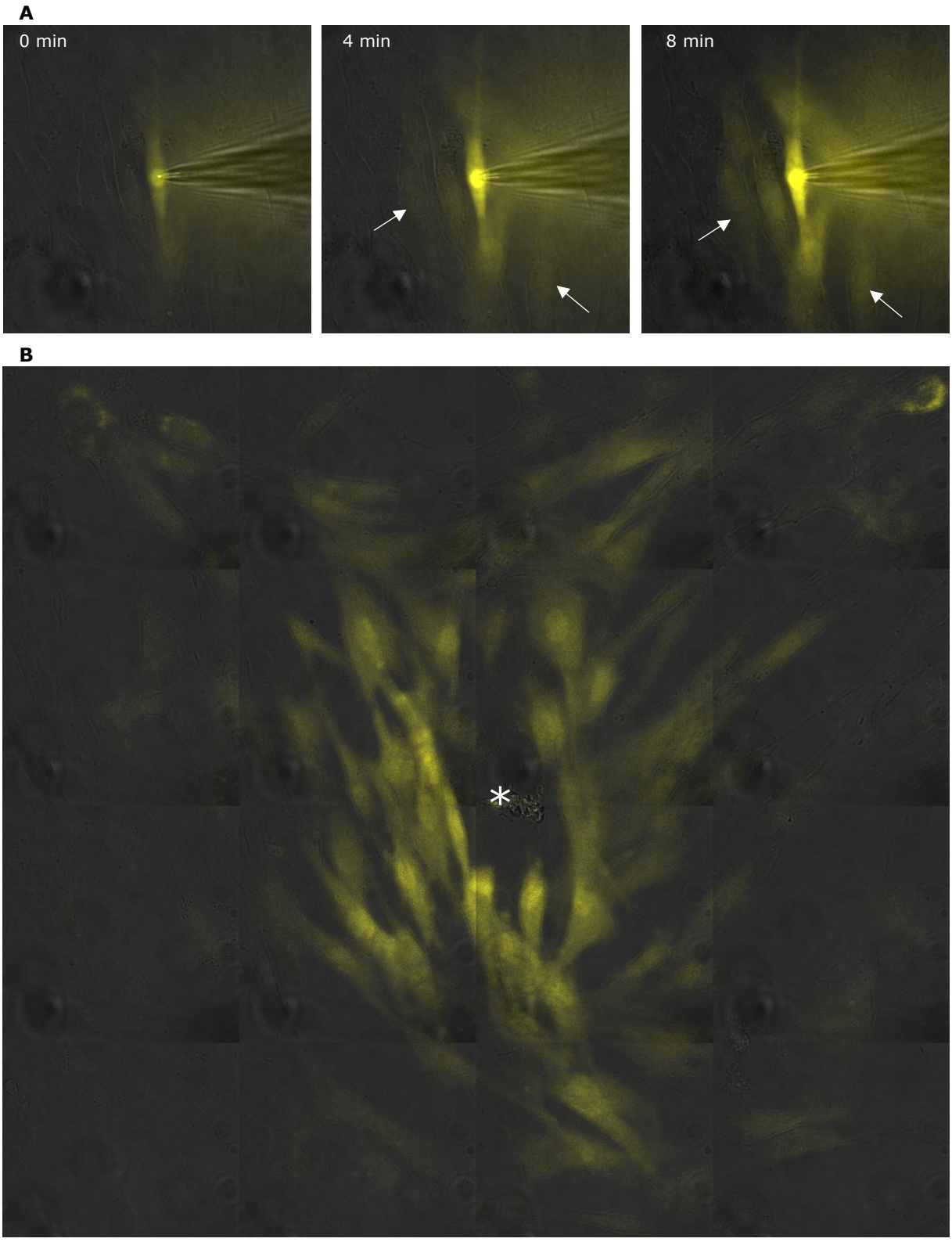

Figure 15 Confirmation of dye coupling of Lucifer Yellow through gap junctions in hDPSCs. A) *In a pilot experiment, hDPSCs are seeded to confluency and left for an additional two days to allow gap junction formation. A yellow staining is visible in the micro-injected DPSC at 0 minutes and the diffusion of the dye is observed as time progresses with increasing diffusion from four to eight minutes after Lucifer Yellow micro-injection. White arrows: hDPSCs connected to the primary injected hDPSC through gap junctions.* ***B)*** *An overview image shows the dye coupling between DPSCs after micro-injection of the initial hDPSC, indicating the potential of micro-injection with Lucifer Yellow to assess gap junction functionality. When the micro pipette is removed to generate this overview image, the micro-injected cell is stuck to the pipette and removed from the petri dish. Abbreviations: OSCC, oral squamous cell carcinoma; hDPSC, human dental pulp stem cells. Asterisk: spot where the initial hDPSC was micro-injected with Lucifer Yellow.*

Next, a co-culture of hDPSCs and OSCC cells are seeded and left to rest identical to the pilot experiment. Single hDPSCs, surrounded by both other hDPSCs as well as OSCC cells are selected and micro-injected with Lucifer Yellow. As time progresses, the fluorescent dye distributes from the primary hDPSC to surrounding cells including OSCC cells (Figure 16A; 4 – 8 min), discernible through their divergent morphology. An overview image of the co-culture shows distribution to surrounding cells to a similar extent than the pilot experiment (Figure 16B).

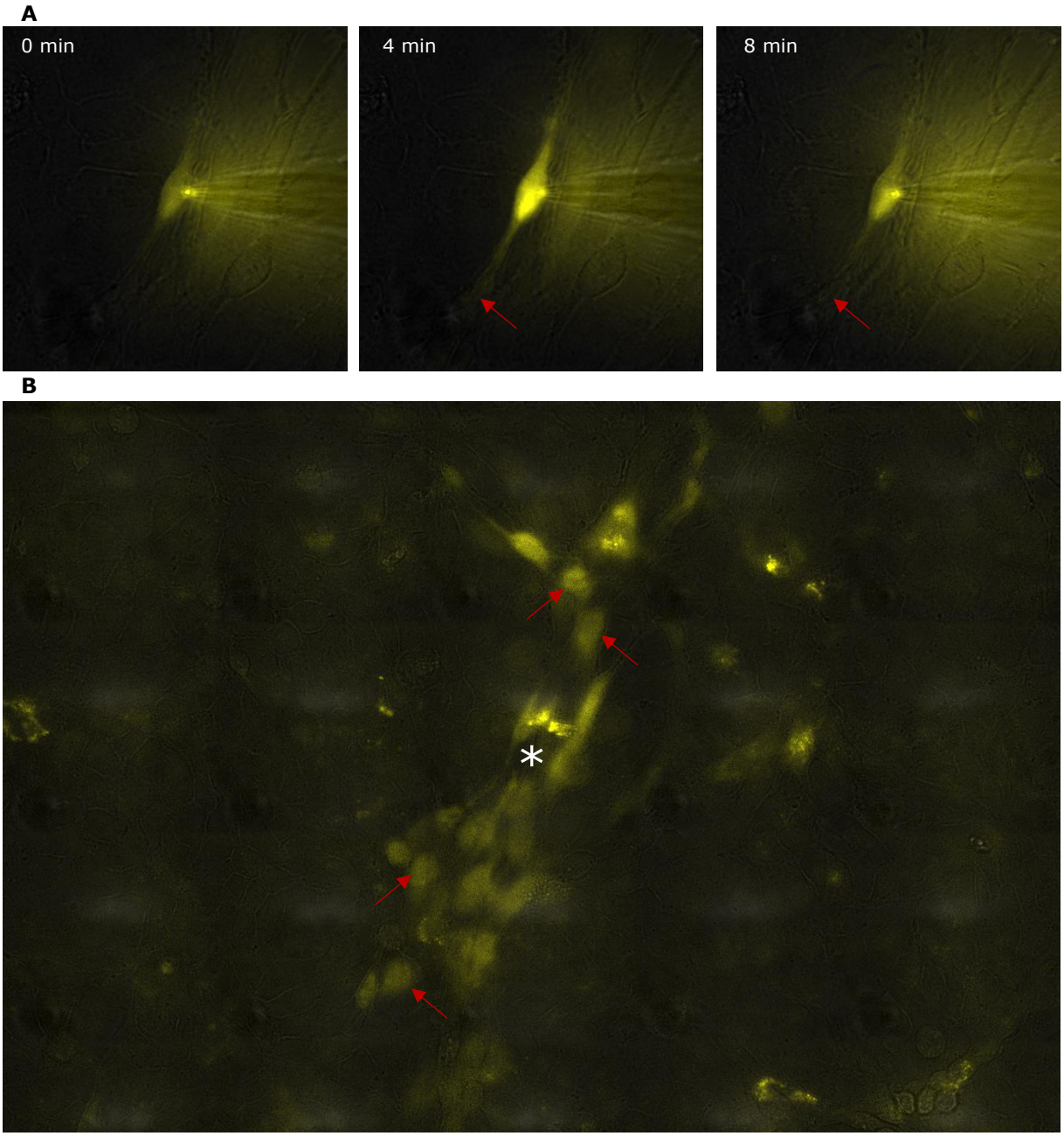

Figure 16 Gap junction functionality confirmation through dye coupling of Lucifer Yellow in a co-culture of hDPSCs and OSCC cells. A) *A co-culture of hDPSCs and OSCC cells, seeded at a ratio of 1:1 to confluency are left for two days to allow gap junction formation. Lucifer Yellow can be observed flowing from the primarily injected hDPSC to surrounding OSCC cells.* ***B)*** *The overview image shows dye coupling between hDPSCs and OSCC cells, indicating that the gap junctions between the two cell cultures are functional. When the micro pipette is removed to generate the overview image, the micro-injected cell, together with some surrounding cells, can be removed due to their attachment to the micropipette. Abbreviations: OSCC, oral squamous cell carcinoma; hDPSC, human dental pulp stem cells. Asterisk: spot where the initial hDPSC was micro-injected with Lucifer Yellow. Red arrows: OSCC cells connected to the primary injected hDPSC through functional gap junctions.*

3.5 Characterization of tumor growth in the 4-nitroquinoline-1-oxide rat model

3.5.1 Histochemical analysis

Rat tongues exposed to 4NQO either through topical administration or through their drinking water ad libitum are stained through a Masson's trichrome staining. Histology is compared to the tongues of healthy control animals. Figure 17A shows a healthy control tongue where the distinct layers of the squamous epithelium can be discerned: stratum corneum, stratum granulosum, stratum spinosum and stratum basalis, from top to bottom respectively, leading to the depiction of a corrugated structure. However, this normal structure appears to be altered after six months of topical 4NQO administration (Figure 17B) as this corrugated structure has disappeared. Animals exposed to 4NQO for four, five, six and eight months through their drinking water (Figure 17C-F, respectively) show a decreasing normal tissue structure with ascending exposure time. At month eight (Figure 17F), tumorous tissue is visible with the naked eye and growths of epithelium are visible in the connective tissue (enlarged image, Figure 17F). Atypia and severe dysplasia are detected from month six (Figure 17E).

The epithelial keratin growths that have invaded the connective tissue can be observed starting from an eight-month time point. Figure 17G-H shows a rat exposed to 4NQO through its drinking water for eight months where the lesion shows a ventral outgrowth of epithelial origin and keratin can be observed in between the strings of connective tissue that are still present (Figure 17G, black arrows). Figure 17H depicts a magnification of the excessive keratin that can be detected in the lesion site where epithelial cells and connective tissue (Figure 17H, black arrows) are interlaced.

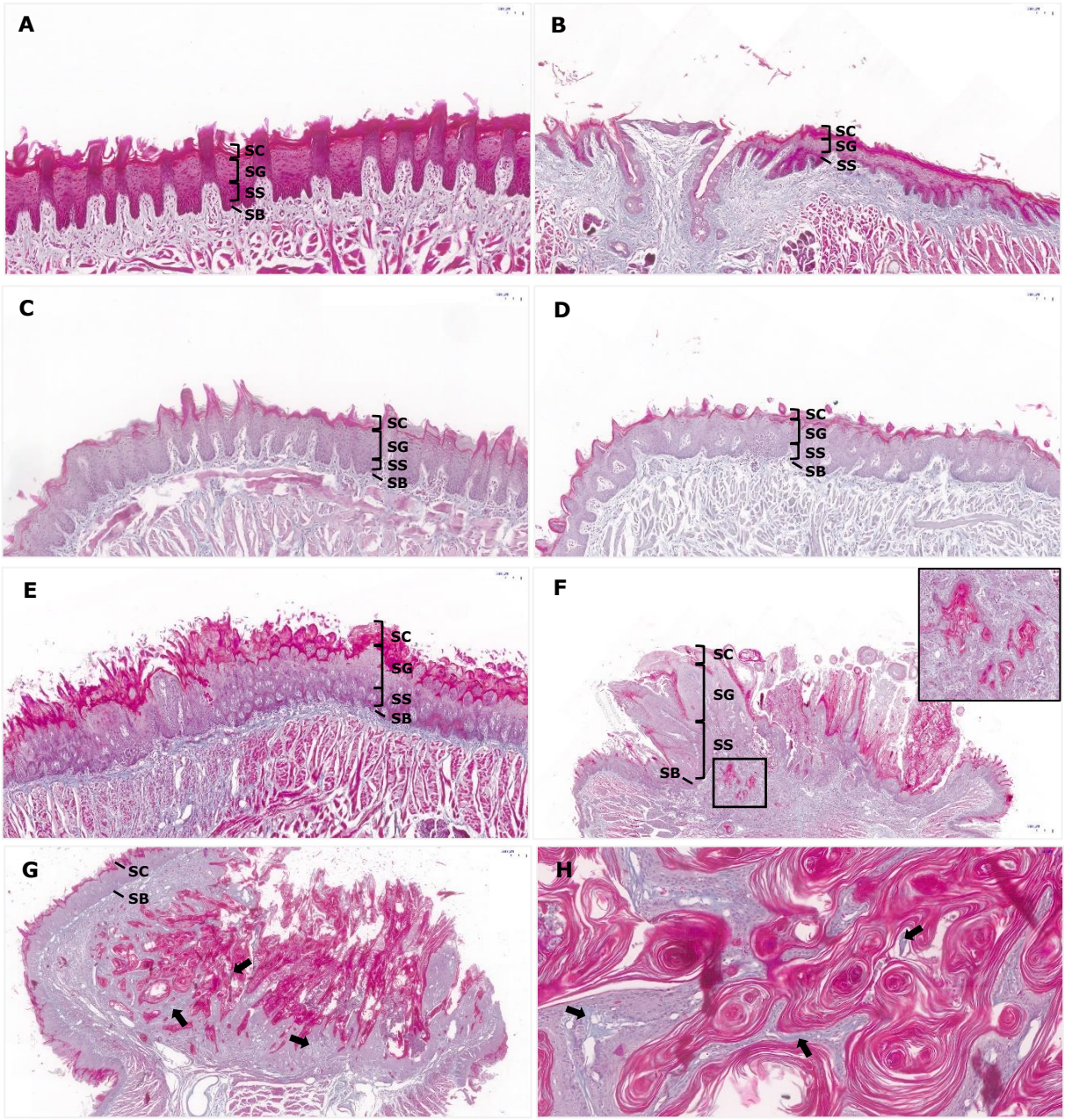

Figure 17 Masson's trichrome staining of tongues of rats exposed to different administration routes of 4NQO for different periods. A) *A healthy control animal depicts the normal histology of the tongue (scalebar 100 µm) and* ***B)*** *8 months of topical administration of 5 mg/mL 4NQO (scalebar 200 µm). Other images depict rat tongues, exposed to 0.01 mg/mL 4NQO through the drinking water of the animals for* ***C)*** *4 months (scalebar 100 µm),* ***D)*** *5 months (scalebar 200 µm),* ***E)*** *6 months (scalebar 200 µm) and* ***F)*** *8 months (scalebar 500 µm; enlarged image scalebar 200 µm). Keratin pearls can be observed intertwined within the connective tissue:* ***G)*** *An overview image of a middle section of an 8-month-old 4NQO-exposed rat shows hyperkeratinization which has infiltrated the underlying connective tissue (black arrows) (scale bar 500 µm) and* ***H)*** *enlarged image of the hyperkeratinization seen dispersed within the connective tissue (black arrows) (scale bar 50 µm). Abbreviations: 4NQO, 4-nitroquinoline-1-oxide; SC, stratum corneum; SG, stratum granulosum; SS, stratum spinosum; SB, stratum basalis.*

3.5.2 Immunohistochemical analysis

To optimize the animal rat model for OSCC in terms of 4NQO administration and exposure time a diverse set of different immunohistochemical markers indicated in OSCC are examined. Rat tongues either exposed to 4NQO topically or administered through the drinking water ad libitum are immunohistochemically assessed through an anti-p63 staining. Tumorous tissue which depicts a p63 staining is of epithelial origin and therefore is indicative to illustrate the presence of OSCC in the 4NQO-exposed rat tongues. Healthy control animals (Figure 18A) show little to no p63 presence, but as exposure time progresses the little p63 staining gets more profound. However, after eight months of 4NQO ad libitum exposure an intense p63 can be seen in the stratum basalis (Figure 18D, enlarged image) as well as in the accessory tumorous growths (Figure 18D, left side of image).

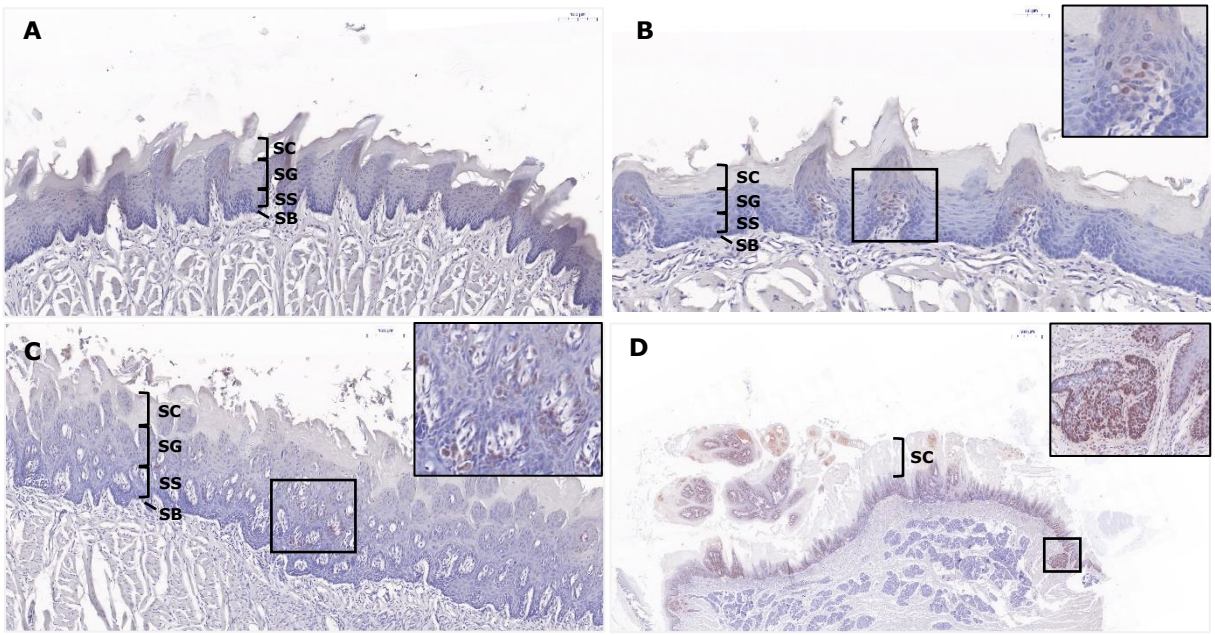

Figure 18 Immunohistochemical analysis of rat tongues exposed to 4NQO with p63. A) *The healthy control shows little to no p63 staining (scale bar 100 µm) while small aggregations of staining are depicted in* ***B)*** *rat tongues exposed to 8 months of topical 5 mg/mL 4NQO administration (scalebar 50 µm; enlarged image 20 µm). Similar aggregations are seen in* ***C)*** *animals exposed through their drinking water (0.01 mg/mL) for 6 months (scalebar 100 µm; enlarged image 50 µm) and a brighter staining is seen at* ***D)*** *8 months exposure through the drinking water (scalebar 50 µm). Abbreviations: 4NQO, 4-nitroquinoline-1-oxide; SC, stratum corneum; SG, stratum granulosum; SS, stratum spinosum; SB, stratum basalis.*

CD44 is associated with the activation of cell signaling pathways that promote cell proliferation and therefore an upregulation in this gene is expected in tumorous tissue. The healthy control animals (Figure 19A) show little CD44 staining on the surface of the filiform papillae and analogous staining is observed as exposure time to 4NQO progresses. However, animals exposed to topically administered 4NQO for six months show a dorsal outgrowth (Figure 19B) with a more intense staining in the stratum granulosum and stratum basalis. Similar staining patterns are seen in the ad libitum 4NQO-administered animals over time (Figure 19C-D) with intense staining in both stratum granulosum and stratum spinosum (Figure 19D) and in the developing tumorous tissue.

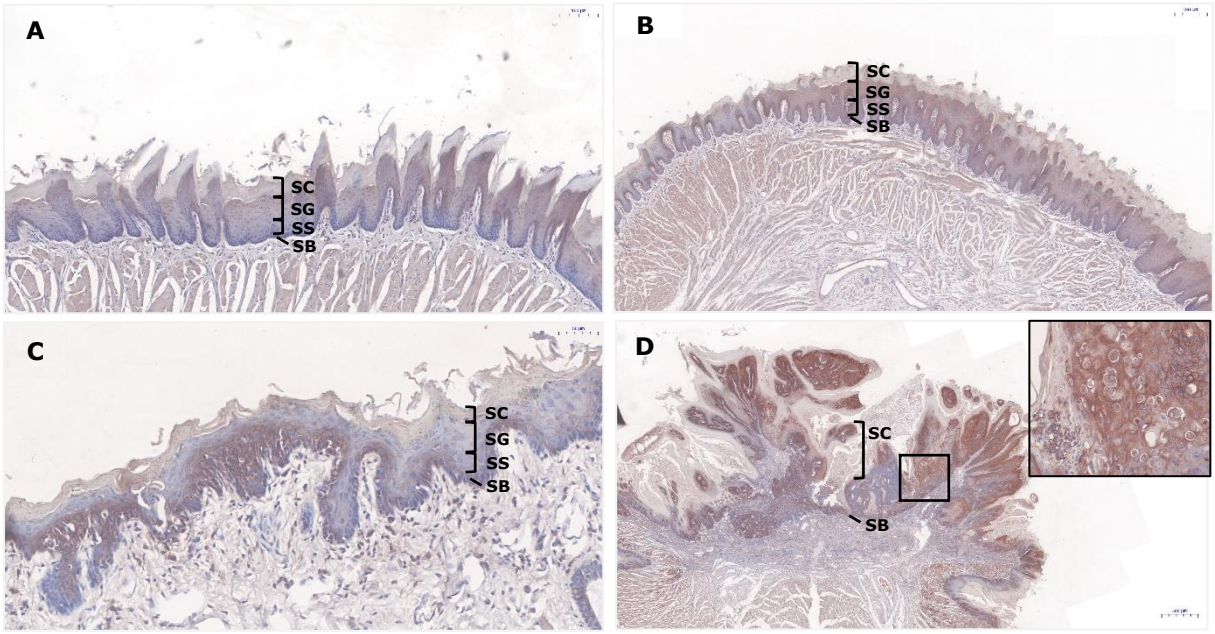

Figure 19 Immunohistochemical analysis with CD44 of rat tongues exposed to 4NQO. ***A)*** *Healthy control slices show little to no specific CD44 staining (scale bar 100 µm) while* ***B)*** *rat tongue slices exposed to 6 months topical 5 mg/mL 4NQO administration (scalebar 200 µm) and* ***C)*** *animals exposed through their drinking water (0.01 mg/mL) for 6 months (scale bar 50 µm) show CD44 presence in the stratum basalis of the epithelium with descending intensity of stain in the stratum spinosum. Visible tumorous tissue is intensely stained for CD44 in* ***D)*** *animals exposed for 8 months through the drinking water (scale bar 500 µm; enlarged image 50 µm). Abbreviations: 4NQO, 4-nitroquinoline-1-oxide; SC, stratum corneum; SG, stratum granulosum; SS, stratum spinosum; SB, stratum basalis.*

Melanoma-associated antigens (MAGEA) are tumor markers with a typical expression pattern observed in a variety of malignant neoplasms such as OSCC. MAGEA-4, and more importantly MAGEA-3, are highly expressed in head and neck cancers. The healthy control animals (Figure 20A) show a background staining which can be attributed to the high blood flow of the tongue tissue. The epithelium is completely disrupted after eight months of topically 4NQO-exposed animals (Figure 20B). Furthermore, an intense staining is observed in the stratum basalis and into the stratum spinosum (Figure 20B, enlarged image). However, with animals exposed to 4NQO ad libitum for six months this intense staining can be observed in the stratum spinosum and stratum granulosum of the epithelial tongue tissue (Figure 20C, enlarged image). Near eight months of ad libitum exposure recurrent staining in the stratum basalis is observed (Figure 20D, enlarged image) with little to no staining in the stratum spinosum or stratum granulosum.

Control sections stained with an antibody against MAGEA-3 show a little background staining in the upper layers of the epithelium (Figure 20E) similar to the animals that were exposed ad libitum to 4NQO for five months (Figure 20G). After eight months topical exposure to 4NQO little MAGEA-3 staining is observed in the stratum basalis. However, after eight months of ad libitum 4NQO exposure intense staining is observed in the outgrowing tumorous tissue (Figure 20H) as well as in the stratum lucidum and stratum granulosum of the tissue surrounding the tumorous outgrowths.

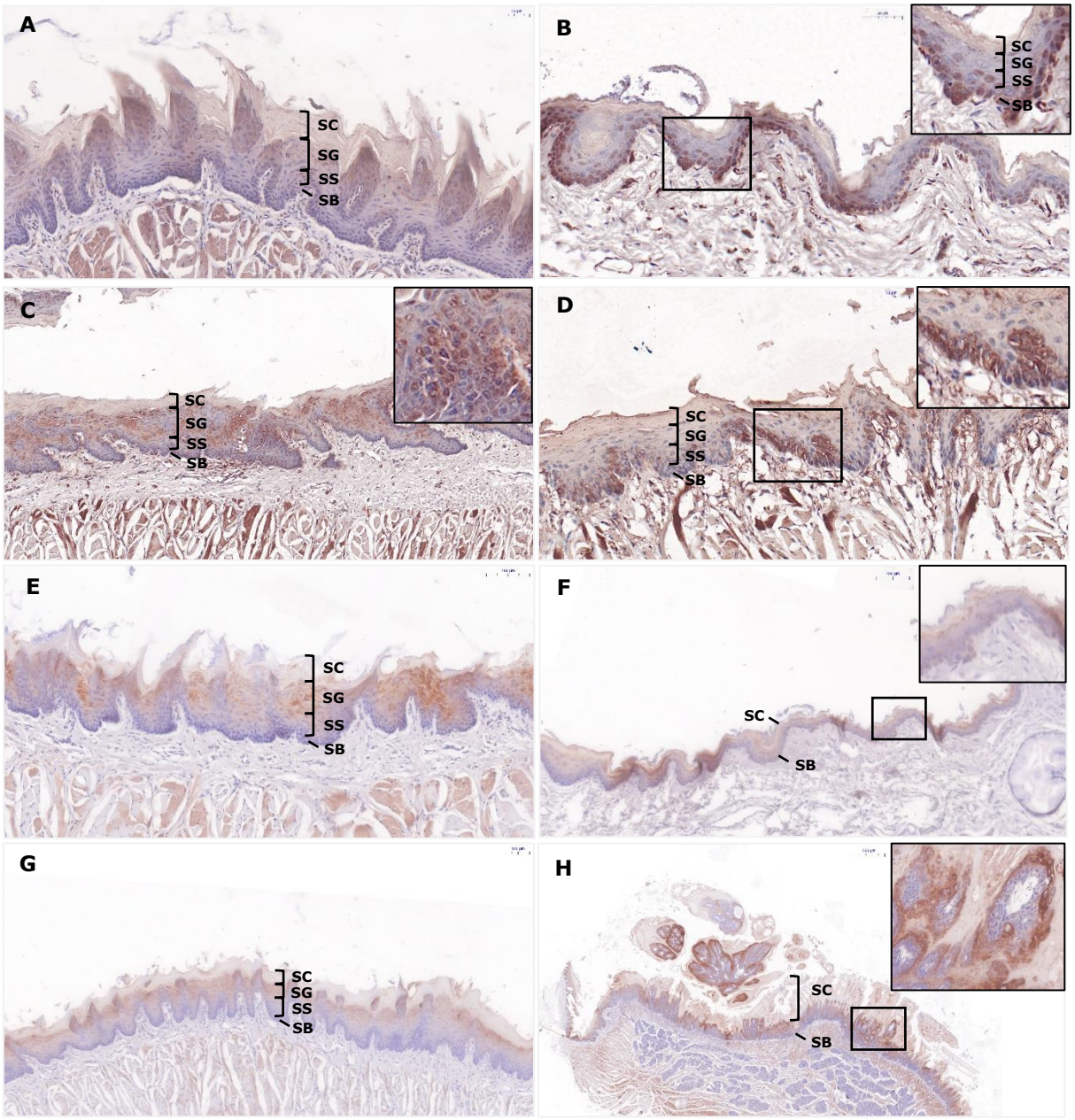

Figure 20 Immunohistochemical analysis of rat tongues exposed to 4NQO with MAGEA-3/4. *Firstly, a MAGEA-4 staining is performed where **A)** the healthy control animal shows little MAGEA-4 staining (scale bar 50 µm) while the stratum basalis shows strong staining in **B)** rat tongues exposed to 8 months of topical (5mg/mL) 4NQO administration (scalebar 50 µm; enlarged image 20 µm). No differences with the control animal can be depicted in **C)** animals exposed through their drinking water (0.01 mg/mL) for 6 months (scale bar 100 µm; enlarged image 20 µm). However, a brighter staining is depicted in the stratum basalis at **D)** 8 months exposure through the drinking water (scale bar 50 µm; enlarged image 20 µm), similar to the local administration route. The MAGEA-3 staining reveals little staining in the stratum granulosum of **E)** healthy control rats (scale bar 100 µm). The stratum corneum and stratum lucidum of **F)** a rat tongue exposed locally for 8 months (scale bar 100 µm; enlarged image 50 µm) and **G)** a rat tongue exposed ad libitum for 5 months (scale bar 100 µm) show little MAGEA-3 staining like the healthy control animal. After **H)** 8 months of ad libitum exposure intense MAGEA-3 staining covers the outer layer of the tumorous outgrowths (scale bar 500 µm; enlarged image 100 µm). Abbreviations: 4NQO, 4-nitroquinoline-1-oxide; SC, stratum corneum; SG, stratum granulosum; SS, stratum spinosum; SB, stratum basalis.*

4 Discussion

Despite major advances in research and therapy for oral squamous cell carcinoma there has been no improvement in the 5-year survival rate and mortality rates remain high (4, 11). Suicide gene therapy with HSV1-sr39-tk as a suicide gene is a potential therapeutic approach; however, the delivery system of the gene to the cancer site remains a major challenge in current suicide gene therapy (24). Viral vectors used to induce the expression of HSV1-sr39-tk is still prevailing, even though they are associated with safety issues and impaired targetability (28, 29). New delivery systems must be investigated and developed to address the adverse effects observed with current delivery systems. Therefore, using human dental pulp stem cells are a carrier for the suicide gene is investigated by our research group. In this project, the focus was to generate a vector that harbors the suicide gene, to assess gap junction presence and functionality and to characterize the 4NQO rat model for further *in vivo* experimentation.

First, to assess hDPSCs as a potential carrier for the suicide gene, they must express the HSV1-sr39-tk gene. Therefore, two plasmids were designed to be introduced into a lentiviral vector thereafter: the EF1-α-HSV1-sr39-tk-T2A-fLuc-IRES-PURO^R plasmid which expresses the HSV1-sr39-tk suicide gene and the fLuc gene for visualization of transduced hDPSCs, and the EF1-α-eGFP-T2A-fLuc-IRES-PURO^R plasmid which expresses the eGFP gene as a control plasmid and the fLuc gene.

Viral vectors have been used in suicide gene therapy and have evolved as vehicles for gene delivery to target cells over the years which led to the application of recombinant viruses such as adenoviruses, adeno-associated viruses, retroviruses and lentiviruses in gene therapy (66). However, ample limitations have persisted such as the instability of the viral particle, the inability to transduce non-dividing cells and insertional mutagenesis. To date, the most applied viral vectors for cancer gene therapy are based on adenoviruses (66, 67). However, they are strongly immunogenic and induce the synthesis of pro-inflammatory cytokines (e.g., IL-6, TNF-α) (67). Furthermore, the transgene expression is temporary and thus susceptible to gene silencing and there are high levels of pre-existing immunity to adenoviruses in the population (68).

Recently, research focused on the use of lentiviral vectors as they have a low probability of gene silencing and can transduce non-dividing cells (66, 69). It is a considerable advantage that the vector genome is integrated into the host cell genome leading to a prolonged expression of the desired transgene. Although there is still a risk for insertional mutagenesis, lower frequencies than with other viral vectors (e.g. oncoretroviral particles) are observed because they integrate further away from cellular promoters (68, 70). Furthermore, there is no pre-existing immunity in the population; rendering them profitable in systemic administration (68). Therefore, to transduce hDPSCs with the HSV1-sr39-tk gene, the research team opted for a lentiviral delivery system to deliver the HSV1-sr39-tk transgene into the hDPSCs.

Additionally, the use of cell type-specific promoters is rewarding as they are less sensitive to promotor inactivation and less expected to activate the defense machinery of the host cell (71). In this project, the EF1-α promoter is present in the already generated plasmid. For stem cells, the EF1-α promoter has been indicated as beneficial in comparison to e.g., cytomegalovirus promoters (72, 73). Therefore, improved stability and longevity of gene expression can be expected (71).

The generation of an experimental plasmid started with introducing HSV1-sr39-tk. The lentiviral vector will deliver this HSV1-sr39-tk suicide gene into the hDPSCs. There are extensively studied systems such as the cytosine deaminase gene of *E. coli* which converts the precursor of the anti-cancer drug 5-flourouracil to its toxic form (15, 32). However, this conversion can also happen in the normal flora of the gut, resulting in adverse effects. Furthermore, the employed bacterial cytosine deaminase has a high affinity for its natural substrate cytosine leading to higher dose requirement (32).

Although the HSV1-tk/GCV mechanism is heavily reliant on the bystander effect, its efficacy *in vitro* had the widest therapeutic index of the four most employed suicide gene prodrug combinations (74). Furthermore, the extensive knowledge on the HSV1-tk/GCV system allows a faster progress to optimize the therapy for OSCC (14, 15, 26, 32). Additionally, important problems in gene therapy are the inability to monitor whether gene transfer is achieved, what tissue is transduced and what the duration of transgene expression is (75). In this project, the distribution and HSV1-sr39-tk transgene expression can be monitored because HSV1-sr39-tk can be used as a reporter gene (15, 16). The radiolabeled analogues of thymidine such as ^{124}I-FIAU can be used as a substrate and evaluate the location and intensity of gene expression *in vivo* (15, 75). Additionally, HSV1-sr39-tk can be employed as a reporter gene with radiolabeled substrates; therefore, the control vector holds the eGFP gene to allow fluorescent visualization of transduced hDPSCs alongside bioluminescent visualization by fLuc.

Moreover, to visualize the plasmid in the hDPSCs *in vitro*, a fLuc gene was added to the plasmid construct. Luciferase is an enzyme that catalyzes a light-producing chemical reaction when luciferin is added, considering the fLuc-expressing cells deliver adenosine triphosphate. This creates a bioluminescent signal that can be detected (76, 77). The generated signal allows for the determination of viral vector presence in the hDPSCs after transduction to select transduced cells from non-transduced hDPSCs and the monitoring of gene expression (77).

When cloning HSV1-sr39-tk in the experimental plasmid, an additional fragment could be observed in the restriction pattern. This was attributed to an incomplete restriction digestion (78) and the plasmid was utilized to proceed to the introduction of the fLuc fragment. Clones that harbored the desired restriction pattern containing both HSV1-sr39-tk and fLuc were selected and used to generate the control plasmid that holds the eGFP gene. However, when introducing the eGFP fragment this additional fragment which was first detected when engineering the HSV1-sr39-tk plasmid was observed in all the samples. Contamination of working solutions (e.g., water, restriction buffers) was excluded by restarting the cloning experiments with new solutions; however, the same restriction pattern persisted. This divergent restriction pattern can be elucidated by ample factors. For example, extra fragments seen on an agarose gel could indicate the partial restriction of the enzyme digest (78). Furthermore, vector closure without uptake of the phosphorylated insert can also appear during the ligation process. Another explanation can be star activity, where the specificity of the restriction enzyme(s) is altered due to suboptimal reaction conditions (78, 79). However, the manufacturer's protocol was meticulously kept.

To progress with *in vitro* studies, a functional experimental and control plasmid must be achieved; therefore, cloning experiments are still ongoing. Additionally, to determine the origin of this additional fragment the generated plasmids can be sequenced to determine divergent DNA sequences in the generated plasmid or the origin of this additional fragment should be determined to eliminate it from further experiments.

An essential aspect of the HSV1-tk/GCV mechanism is the conversion of ganciclovir to its toxic, triphosphorylated metabolite that induces apoptosis in 3P-GCV-containing cells (14). However, another important feature is the bystander effect as 3P-GCV exerts an amplified effect via gap junctions (14, 80). Although the significance of the bystander effect is partially bypassed by administering ample hDPSCs, gap junctions are crucial to achieve a satisfactory amount of cancer cell killing (81). Therefore, gap junction presence and functionality were assessed.

Connexin-43 is an abundant protein in gap junction channels of ample cell types to allow diffusion of small molecules (81, 82). Cx-43 is found not only in gap junctions but also in the cell membrane. Results indicate that Cx-43 expression is more pronounced in cell-dense regions and where the cells are making contact. This Cx-43 expression is an indication of gap junction presence (83). The existence of these gap junctions between hDPSCs and OSCC cells and between OSCC cells is an essential feature for the bystander effect (81, 84). However, they also must be functional to investigate HSV1-tk suicide gene therapy with hDPSCs.

First, the dye coupling principle of Lucifer Yellow was evaluated in a hDPSC cell culture. Dye coupling is the movement of a dye molecule from cell to cell which are connected through functional gap junctions (85, 86). Gap junctions allow the passage of small molecules which have a molecular weight smaller than 1000 Dalton (Da) (87). Lucifer Yellow is a fluorescent molecule that behaves similarly as the prodrug ganciclovir as it does not diffuse through intact plasma membranes and has a molecular weight of 457.3 Da (86). The dye coupling observed between hDPSCs is a proof of principle that Lucifer Yellow can visualize gap junction functionality *in vitro* (88). After approximately nine minutes no more diffusion of dye was observed. Research elucidated that dye coupling could be observed up until ten minutes (89, 90); however, after the ten-minute-limit had passed no changes in dye coupling could be observed up until three hours after micro-injection (90). Therefore, further co-culture experiments with Lucifer Yellow can be terminated ten minutes after micro-injection.

Although hDPSCs and OSCC cells are visually distinguishable through their morphology (9, 45), hDPSCs and OSCC cells were stained in the co-culture to allow easy determination of cell type for further Lucifer Yellow micro-injection with CD90 and EpCAM, respectively. CD90 is a cell adhesion molecule that is anchored to the cell surface and is expressed on human dental pulp stem cells (46, 91) and has been indicated to play a role in growth and differentiation of stem cells (91). Meanwhile, EpCAM is an epithelial cell adhesion molecule found in the lateral cell membrane that is involved in the calcium-independent homotypic cell-cell adhesion in epithelial tissues and is overexpressed in various cancer types (92). EpCAM expression is absent in normal oral mucosa but present in 85% of OSCC cases (93). Results indicated that either antibody was specific against the cell adhesion molecules respectively, and thus potentially employable in the dye coupling experiments to visually distinguish hDPSCs and OSCC cells from one another.

Staining hDPSCs in a live, non-fixed co-culture with the marker against CD90 rendered the cells less viable; in the co-cultures seeded for dye coupling experimentation and stained against CD90 significantly more cell death was observed compared to co-cultures seeded at the exact same time and visualized the same day. Other staining possibilities, such as transfection of these hDPSCs with an eGFP gene might be more suitable to distinguish hDPSCs from OSCC cells for dye coupling experimentation (94).

Next, hDPSCs were micro-injected for dye coupling analysis to confirm one of the pillars of suicide gene therapy. Lucifer Yellow dye coupling was observed, indicating functional gap junction presence between hDPSCs and OSCC cells. Therefore, an important pillar of suicide gene therapy, the bystander effect, can occur in *in vitro* co-culture experiments. However, when limited dye coupling is discerned full confluency and gap junction formation must be achieved.

Furthermore, after completion of the *in vitro* studies, *in vivo* experimentation will be initiated. The 4NQO model is the most used chemical carcinogen-induced model worldwide (95). The multi-step approach of oral cancer induction is an advantage of the 4NQO model (59, 95) as the development of malignant OSCC is preceded by increasing grades of dysplastic alterations which mimic oral cancer development in humans (59). Research indicated that 100% of 4NQO-administered mice exhibit precancerous lesions which result in tumors on the tongues and oral mucosa (96, 97). However, the size of a mouse's tongue and the induced lesion size can pose issues in visualization when imaged with MRI. Furthermore, OSCC induced in rats by 4NQO show morphological and histopathological similarities to human OSCC (98).

In this selected 4NQO *in vivo* rat model suicide gene therapy with HSV1-sr39-tk-transduced hDPSCs as a carrier will be assessed. Therefore, tumor growth and size were evaluated to select the optimal model and 4NQO exposure time before starting with therapy. Two exposure methodologies were evaluated: in the drinking water of the animals and applied onto the tongue after anesthesia.

The corrugated structure observed in the control animals disappears as exposure time to 4NQO progresses in animals exposed through their drinking water. An important hallmark observed in the 4NQO-exposed drinking water group of animals is the disruption of the stratum basalis, as it indicates the start of the invasion process (99). The morphological changes such as dyskeratosis that is visible in the tongue epithelium of 4NQO drinking water-exposed animals show high differentiation of the cancer tissue. Dyskeratosis is defined as abnormal keratin production, which is often depicted as individually keratinizing lesion sites or keratin pearls (100) and is also an indication of invasion into the connective tissue (101, 102). The amount of malignant keratinization also suggests the grade of malignancy in OSCC (100, 103). Therefore, eight months of 4NQO exposure through the drinking water appears too extensive.

Further characterization was performed through immunohistochemical evaluation of an assorted set of markers: p63, CD44, MAGEA-3/4, p53 and Ki-67. In some samples, intense staining is observed of the muscle tissue of the tongue. The primary functions of the tongue are mastication and deglutition. Therefore, the tongue is strongly innervated and highly vascularized which causes more endogenous peroxidase presence (104) leading to a certain amount of background staining even when peroxidase blocking is performed. Furthermore, paraffin sectioning regards a sufficient tissue

structure but causes a loss in antigenicity due to high temperatures and the formalin fixation employed during embedding procedures (105).

One of the selected markers was p63, which is a well-known marker for squamous differentiation that is localized in the nucleus. It has an important role in cell cycle regulation and tumor differentiation (106). A positive p63 staining is predictive of squamous epithelial origin and has been shown to be expressed in the stratum basalis of the normal oral mucosa with an increased expression in head and neck squamous cell carcinoma (106-108). As 4NQO exposure time progresses and outgrowths become discernible p63 staining intensifies indicating that the tumorous tissue is of epithelial origin (108).

CD44 is a cell surface adhesion receptor that resides in the cellular membrane which upon activation by its main ligand hyaluronan results in the activation of cell signaling pathways. This activation additionally induces cell proliferation, increases cell survival and enhances cellular motility (109, 110). Tumors of epithelial origin express different isoforms of CD44 such as isoform 10 (CD44v10) and is also highly expressed in carcinomas (110). The antibody employed to evaluate OSCC in the rat tongues was directed against CD44v10 and its staining increased as exposure to 4NQO progressed and tumorous outgrowths were distinguished. Strong expression of CD44v10 is associated with shorter disease-free survival in primary tumors as well as higher chances of failure of radiotherapy (110). CD44 and p63 are identified as markers in normal squamous epithelium and SCC (106). An increased expression of both p63 and CD44 as observed in the immunohistochemical analysis of 4NQO-exposed histological slices is correlated with advancement in the tumor grade and stage of oral squamous cell carcinoma (106, 111).

Next, MAGEA was evaluated. The MAGEA family is activated in a variety of neoplasms but they are absent in healthy normal tissues except the testis. Therefore, it is an attractive target in cancer detection such as the oropharyngeal regions in head and neck carcinomas (112). A more intense staining of MAGEA-4 that is seen as 4NQO exposure time progresses (e.g., around seven and eight months) in the drinking water-exposed group is associated with a higher tumor grade and stage of OSCC (112, 113). Most MAGEA antigens such as MAGEA-4 are expressed in OSCC; however, MAGEA-3 is one of the predominantly expressed antigens (114). MAGEA-3 plays a prominent role in growth promotion; indicating its importance in tumor transformation and tumor progression (114, 115). Ascending staining intensity in MAGEA-3 as seen with the drinking water group in the stratum granulosum and stratum lucidum or the tumorous outgrowths that are intensely stained in various histological slices indicate progression and transformation from normal growth to malignancy (115).

p53 is a tumor suppressor gene that when mutated leads to promotion of cell cycle progression and thus, can cause uncontrolled cell growth (116). This protein is commonly found in human cancer such as OSCC (117). Results indicate no significant p53 staining in the histological slices. The monoclonal antibody employed to visualize p53 recognized both mutant and wild type conformational forms under denaturing conditions. However, under conventional circumstances the histological slices are not denatured during the immunohistochemical staining protocol. Therefore, more intense antigen retrieval was performed which denatures the paraffin-embedded slices slightly (118). In comparison to the standard employed antigen retrieval a p53 staining was detected; however, no

distinct staining could be observed in the nuclei even though p53 is a nuclear marker. There is also a possibility that the used antibody is not suitable for immunohistochemistry evaluation.

Cell proliferation is considered one of the most essential mechanisms behind oncogenesis. Ki-67 is present in all proliferating cells but absent in resting cells. Therefore, it is used as a marker to examine the proportion of proliferating cells in neoplasms (119, 120). Ki-67 is a peptide that is expressed during the G1, S and G2 phases of the cell cycle and is localized in the nucleus (120). However, apart from the observed outgrowths little staining is observed. Ki-67 should be visible in the healthy control animals in the stratum basalis of the epithelium as these cells are continuously proliferating to replace the outer layer of the skin. Furthermore, an intense staining is also expected in tumorous outgrowths as one of the hallmarks of cancer is uncontrolled proliferation (2) and a higher percentage of Ki-67 is correlated with advanced histologic grading in OSCC (120). One option is that the fixation of the tongue tissue led to cross-linking and thus, the antigens are masked (121). Therefore, a more intense antigen retrieval as was tried with p53 should be attempted.

When the two experimental administration groups are compared to one another, the ad libitum drinking water group shows greater formation of tumor tissue as well as a higher degeneration of the normal structure of the epithelium than the topically administered group at identical exposure time. Another possibility includes the steeper increase of tumorous tissue in a shorter time period (122) as more animals of the local administration group died in comparison to the ad libitum group. Another explanation is that the saliva of these rats has a protective role against carcinogens; Kaplan *et al*. showed that saliva has a temporary anti-carcinogenic protective effect that can delay and decrease the proliferation levels induced by 4NQO (123). This can lead to a delay of tumor development in the topically 4NQO-administered group. Additionally, it is also possible that the tumor tissue present in these rat tongues was not sliced for analysis. However, none of the tested topically 4NQO-administered animals demonstrated tumorous outgrowths rendering this issue implausible.

Furthermore, one of the primary goals of these experiments is to limit the suffering of the animal. The topically 4NQO-administered animals were anesthetized three times per week to apply the carcinogen; this leads to additional stress and together with the observed results renders this experimental group unsuitable from an ethical and experimental perspective.

Applying the carcinogen 4NQO through the drinking water has some advantages. Animals do not have to be anesthetized, which has an impact on stress levels of the animal but also its physiological parameters and can lead to death of the animal (124). Furthermore, limited handling of the animals is necessary when applying 4NQO through the drinking water. Additionally, Ohne *et al.* showed that tumor development was not observed in other major organs such as the upper digestive tract when applying 4NQO through the drinking water (125).

However, lesion size and exposure time to 4NQO must also be determined. Near three months of ad libitum administration the epithelium is dysplastic and disrupted without apparent tumor tissue formation. Ribeiro *et al*. showed that primary histopathological changes could be observed after three months of 4NQO administration (95). However, dysplasia is insufficient as the HSV1-sr39-tk-transduced hDPSCs are injected intratumorally; therefore, tumor formation should be visibly manifested.

Furthermore, at eight months 4NQO exposure through the drinking water apparent tumorous tissue had manifested and ventral outgrowth was discernible indicating invasion into the connective tissue. Extensive local invasion is usually present at initial diagnosis of human OSCC which results in the unpredictable prognosis (126). However, as this extensive local invasion is usually painful and due to the large tumor growths observed in the histological slices eight months of 4NQO exposure through the drinking water was deemed too protracted. The main goal of this project is to assess a reduction of tumor size with a limited suffering for the animals.

Morphological and immunohistochemical analysis indicated six to seven months of 4NQO exposure through the drinking water to be ideal to start treatment; MAGEA-3/4, p63 and CD44 indicated presence of tumorous tissue and histochemical evaluation indicated the discernibility of this tumorous tissue while no invasion into the connective tissue was apparent. Hawkins *et al*. and Knudsen *et al*. indicated that OSCC was detected between three and eight months when 4NQO was applied via the drinking water (59, 127). Wallenius *et al*. showed that 4NQO dissolved in the water produced palatal cancers in all experimental rats by seven months (128). Foy *et al*. described that 100% of 4NQO-administered mice exhibited precancerous lesions and tumors on the tongues and oral mucosa after six to seven months (96) while Ohne *et al*. described that after seven months exposure approximately 70% of rats had developed OSCC (125). Therefore, observed results correlate with existing literature and six to seven months of 4NQO exposure through the drinking water is acceptable to start our proposed therapy.

As one of the most essential routes of human carcinogens that induce OSCC is through liquid-containing water-soluble carcinogens (95), six to seven months of 4NQO administration through the drinking water is ideal to evaluate the potential of HSV1-sr39-tk-transduced hDPSCs as a carrier for suicide gene therapy.

5 Conclusion and synthesis

In 2018, 350.000 new cases were diagnosed with cancer of the oral cavity and/or oropharynx and incidence rates remain ascending in preceding years. The treatment of OSCC is still inadequate due to severe complications and the prominent risk of tumor recurrence. The impact of oral cancer even after treatment results in severely reduced quality of life for survivors. This highlights the need for research and development of novel therapies with a total tumor elimination and a limited loss of healthy tissue.

Ample studies have focused on suicide gene therapy with the HSV1-tk suicide gene as a potential therapy for cancer both *in vitro* and *in vivo*. To date, suicide gene delivery has mainly been done through viral vectors; this hampers the clinical application of this mechanism due to safety issues associated with the use of viral vectors as well as suboptimal delivery systems. The bottleneck of most research is the delivery of the suicide gene where a low percentage of transduced tumor cells is observed.

Therefore, a cellular vehicle that carries the genetic material to the pathology site is necessary; previous research has employed e.g., BM-MSCs due to their inherent migration ability towards the tumor. However, their isolation is arduous and thus, hDPSCs are a more promising and beneficiary approach to the use of cellular vehicles to assist in the HSV1-sr39-tk/GCV mechanism; they are a subtype of MSCs and are isolated from the dental pulp of third molars that are considered waste material once extracted. Furthermore, reports on hDPSCs in similar experimentation is lacking. Consequently, the research group inquired if HSV1-sr39-tk-transduced hDPSCs results in the death of OSCC cells through the bystander effect and subsequently leads to a reduction in tumor size.

The HSV1-sr39-tk suicide transgene is successfully introduced into the plasmid; however, the control plasmid, containing eGFP, is not yet finished. The additional fragment seen in all the restriction patterns needs to be eliminated to ensure a functional experimental and control vector to continue *in vitro* studies. Further trouble shooting is recommended to finish both the experimental and control plasmid for further *in vitro* and *in vivo* experimentation.

Gap junction presence is shown both between hDPSCs and OSCC cells and between OSCC cells. Gap junction functionality is elucidated, assisting in the proof of concept of suicide gene therapy. Dye coupling is not only seen from the primarily injected cell towards adjacent, connected cells; this indicates a connected network the hDPSCs form with the OSCC cells.

Characterization of the 4NQO rat model indicates the ad libitum 4NQO drinking water model is the most optimal; the most fitting start for suicide gene therapy *in vivo* is at approximately 6 – 7 months of exposure to 0.01 mg/mL 4NQO through the drinking water of the animals.

Consequently, the HSV1-tk/GCV mechanism in hDPSCs in a co-culture with OSCC cells and the associated bystander effect could not be demonstrated yet. However, the gap junction presence and functionality, which is one of the pillars of suicide gene therapy, are confirmed.

Continuing, a next advance is to successfully clone either the HSV1-sr39-tk or the eGFP construct into the pSINc plasmid. Both the experimental vector harboring HSV1-sr39-tk and the control vector containing eGFP must be completed to progress *in vitro*. Furthermore, additional dye-coupling experiments between hDPSCs and OSCC cells are required to ascertain gap junction functionality. These results will provide proof of concept for the pillar of suicide gene therapy, namely the bystander effect.

For further *in vitro* experiments, the expression of the HSV1-sr39-tk gene must be evaluated and the functionality of the viral thymidine kinase to monophosphorylate GCV must be validated. Once validated, the optimal GCV dose is determined to successfully eradicate all the transduced DPSCs and OSCC cells in a co-culture.

Moreover, more rat tongue sections of animals exposed via either approach require further (immuno)histologically evaluation to characterize and optimize the 4NQO rat model optimally. Additionally, other antibodies for p53 and Ki-67 should be examined as these markers are commonly employed in human cancer pathology evaluation. A combination of p63 and Ki-67 is employed as an accomplished marker for squamous epithelial cancers. Other markers such as the epidermal growth factor receptor that has been shown to be important in OSCC and its progression should also be assessed to grant a definite and detailed evaluation of the 4NQO rat model.

When *in vitro* experiments and *ex vivo* analyses are finished, *in vivo* evaluation can start. First, the biodistribution and survival of HSV1-sr39-tk-transduced hDPSCs needs to be evaluated in the 4NQO drinking water rat model. The optimal transplantation site as well as the optimal number of injected hDPSCs can then be determined. Afterward, the hDPSC-mediated HSV1-sr39-tk/GCV mechanism can be validated as a therapeutic approach for OSCC.

Suicide gene therapy with hDPSCs as a carrier for the suicide gene towards OSCC cells could improve the 5-year survival rate of OSCC patients and tackle the adverse effects observed with current treatment methodology; there would be no need for resection of large parts of the oral floor and/or tongue, while limiting the loss of healthy normal tissue. Additionally, our therapy could eliminate adverse effects seen with radio- and chemotherapy such as therapy-induced xerostomia. Furthermore, the use of hDPSCs as a carrier could address the limitations observed with current suboptimal delivery systems such as viral vectors.

Preceding experiments indicate the potential of hDPSCs as a carrier in suicide gene therapy. Further research will elucidate the efficiency of hDPSC-mediated suicide gene therapy both *in vitro* as well as *in vivo*.

References

1. WHO. Detailed fact sheet about cancer. World Health Organization; 2018 12/09/2018.
2. Hanahan D, et al. Hallmarks of cancer: the next generation. cell. 2011;144(5):646-74.
3. Bray F, et al. Global cancer statistics 2018: GLOBOCAN estimates of incidence and mortality worldwide for 36 cancers in 185 countries. CA: a cancer journal for clinicians. 2018.
4. Benzian H, et al. The challenge of oral disease: a call for global action. The oral health atlas 2nd ed Geneva: FDI World Dental Federation. 2015.
5. Petti S. Lifestyle risk factors for oral cancer. Oral oncology. 2009;45(4-5):340-50.
6. Herrero R, et al. Human papillomavirus and oral cancer: the International Agency for Research on Cancer multicenter study. Journal of the Cancer Institute. 2003;95(23):1772-83.
7. Kumar V, et al. Robbins basic pathology e-book: Elsevier Health Sciences; 2017.
8. Rivera C. Essentials of oral cancer. International journal of clinical and experimental pathology. 2015;8(9):11884.
9. Lowe JS, et al. Stevens & Lowe's Human Histology E-Book: With STUDENT CONSULT Online Access: Elsevier Health Sciences; 2014.
10. Feller L, et al. Oral squamous cell carcinoma: epidemiology, clinical presentation and treatment. Journal of cancer therapy. 2012;3(04):263.
11. Massano J, et al. Oral squamous cell carcinoma: review of prognostic and predictive factors. Oral surgery, oral medicine, oral pathology, oral radiology, and endodontology. 2006;102(1):67-76.
12. Omura K. Current status of oral cancer treatment strategies: surgical treatments for oral squamous cell carcinoma. International journal of clinical oncology. 2014;19(3):423-30.
13. Minhas S, et al. Concomitant-chemoradiotherapy-associated oral lesions in patients with oral squamous-cell carcinoma. Cancer biology & medicine. 2017;14(2):176.
14. Dey D, et al. Suicide gene therapy by herpes simplex virus-1 thymidine kinase (HSV-TK). Targets in Gene Therapy: InTech; 2011.
15. Zarogoulidis P, et al. Suicide gene therapy for cancer–current strategies. 2013;4.
16. Yaghoubi SS, et al. Positron emission tomography reporter genes and reporter probes: gene and cell therapy applications. Theranostics. 2012;2(4):374.
17. Soghomonyan S, et al. Molecular PET imaging of HSV1-tk reporter gene expression using [18 F] FEAU. Nature protocols. 2007;2(2):416.
18. Boerman OC, et al. FIAU: from reporter gene imaging to imaging of bacterial proliferation. American journal of nuclear medicine and molecular imaging. 2012;2(3):271.
19. Tan BH. Cytomegalovirus treatment. Current treatment options in infectious diseases. 2014;6(3):256-70.
20. Aasen T, et al. Gap junctions and cancer: communicating for 50 years. 2016;16(12):775.
21. Frank DK, et al. Connexin expression and gap junctional intercellular communication in human squamous cell carcinoma of the head and neck. Head & Neck Surgery. 2006;135(5):736-43.
22. Yamasaki H. Gap junctional intercellular communication and carcinogenesis. Parallels in Cell to Cell Junctions in Plants and Animals: Springer; 1990. p. 115-27.
23. Kay MA, et al. Viral vectors for gene therapy: the art of turning infectious agents into vehicles of therapeutics. Nature medicine. 2001;7(1):33.
24. Hatefi A, et al. Perspectives in vector development for systemic cancer gene therapy. Gene therapy & molecular biology. 2009;13(A):15.
25. Kane JR, et al. Sui generis: gene therapy and delivery systems for the treatment of glioblastoma. Neuro-oncology. 2015;17(suppl_2):ii24-ii36.
26. Gambhir SS, et al. A mutant herpes simplex virus type 1 thymidine kinase reporter gene shows improved sensitivity for imaging reporter gene expression with positron emission tomography. Proceedings of the National Academy of Sciences. 2000;97(6):2785-90.
27. Thomas CE, et al. Progress and problems with the use of viral vectors for gene therapy. Nature Reviews Genetics. 2003;4(5):346.
28. Schlimgen R, et al. Risks associated with lentiviral vector exposures and prevention strategies. Journal of occupational and environmental medicine. 2016;58(12):1159.
29. David RM, et al. Viral vectors: the road to reducing genotoxicity. 2017;155(2):315-25.
30. Panghal Archna SH, Flora SJS, Naqvi Saba. Suicide gene therapy: a promising approach towards gene delivery. Front Nanosci Nanotech 5. 2018.
31. Perez-Martinez FC, et al. The use of nanoparticles for gene therapy in the nervous system. Journal of Alzheimer's Disease. 2012;31(4):697-710.
32. Karjoo Z, et al. Progress and problems with the use of suicide genes for targeted cancer therapy. Advanced drug delivery reviews. 2016;99:113-28.
33. Roacho-Perez JA, et al. Nanoparticles for death-induced gene therapy in cancer. Molecular medicine reports. 2018;17(1):1413-20.
34. Seow Y, et al. Biological gene delivery vehicles: beyond viral vectors. 2009;17(5):767-77.

35. Larsen M, et al. Bactofection of lung epithelial cells in vitro and in vivo using a genetically modified Escherichia coli. Gene therapy. 2008;15(6):434.
36. Smalheiser NR. Exosomal transfer of proteins and RNAs at synapses in the nervous system. Biology direct. 2007;2(1):35.
37. Kosaka H, et al. Therapeutic effect of suicide gene-transferred mesenchymal stem cells in a rat model of glioma. Cancer gene therapy. 2012;19(8):572.
38. Kim SU. Neural stem cell-based gene therapy for brain tumors. 2011;7(1):130-40.
39. Duarte S, et al. Suicide gene therapy in cancer: where do we stand? 2012;324(2):160-70.
40. Mahla RS. Stem cells applications in regenerative medicine and disease therapeutics. International journal of cell biology. 2016;2016.
41. de Lucas B, et al. Importance and regulation of adult stem cell migration. Journal of cellular and molecular medicine. 2018;22(2):746-54.
42. Ankrum JA, et al. Mesenchymal stem cells: immune evasive, not immune privileged. Nature biotechnology. 2014;32(3):252.
43. Kim HJ, et al. Usage of human mesenchymal stem cells in cell-based therapy: advantages and disadvantages. Development & reproduction. 2017;21(1):1.
44. Attoumani H, et al. Immune Properties of Human Dental Pulp Stem Cells and Interactions with the Immune System. Ann Stem Cell Res Ther 2018; 2 (3).1018.
45. Hilkens P, et al. Effect of isolation methodology on stem cell properties and multilineage differentiation potential of human dental pulp stem cells. Cell & tissue research. 2013;353(1):65-78.
46. Ashri NY, et al. Dental pulp stem cells: Biology and use for periodontal tissue engineering. Saudi Medical Journal. 2015;36(12):1391.
47. Nuti N, et al. Multipotent differentiation of human dental pulp stem cells: a literature review. Stem Cell Reviews and Reports. 2016;12(5):511-23.
48. Almofti A, et al. The clinicopathological significance of the expression of CXCR4 protein in oral squamous cell carcinoma. International journal of oncology. 2004;25(1):65-71.
49. Li M, et al. SDF-1/CXCR4 axis induces human dental pulp stem cell migration through FAK/PI3K/Akt and GSK3β/β-catenin pathways. Scientific Reports. 2017;7:40161.
50. Gwendal L. Recent discoveries concerning the tumor-mesenchymal stem cell interactions. Biochimica et Biophysica Acta (BBA)-Reviews on Cancer. 2016;1866(2):290-9.
51. Sorrentino C, et al. Activation of the A2B adenosine receptor in B16 melanomas induces CXCL12 expression in FAP-positive tumor stromal cells. Oncotarget. 2016;7(39):64274.
52. Daly AJ, et al. Regulation of HGF and SDF-1 expression by oral fibroblasts–implications for invasion of oral cancer. Oral oncology. 2008;44(7):646-51.
53. Jiang H-w, et al. The Expression of Stromal Cell–derived Factor 1 (SDF-1) in Inflamed Human Dental Pulp. Journal of Endodontics. 2008;34(11):1351-4.
54. Chang J, et al. NF-κB activation in human dental pulp stem cells by TNF and LPS. Journal of dental research. 2005;84(11):994-8.
55. Tomic S, et al. Immunomodulatory properties of mesenchymal stem cells derived from dental pulp and dental follicle are susceptible to activation by toll-like receptor agonists. Stem cells and development. 2010;20(4):695-708.
56. Ishida K, et al. Current mouse models of oral squamous cell carcinoma: Genetic and chemically induced models. Oral oncology. 2017;73:16-20.
57. Schoop RA, et al. A mouse model for oral squamous cell carcinoma. 2009;40(3):177.
58. Arima Y, et al. 4-Nitroquinoline 1-oxide forms 8-hydroxydeoxyguanosine in human fibroblasts through reactive oxygen species. Toxicological Sciences. 2006;91(2):382-92.
59. Hawkins BL, et al. 4NQO carcinogenesis: a mouse model of oral cavity squamous cell carcinoma. Head & neck. 1994;16(5):424-32.
60. Kanojia D, et al. Alterations in keratins and associated proteins during 4-Nitroquinoline-1-oxide induced rat oral carcinogenesis. Journal of carcinogenesis. 2012;11.
61. Nonaka T, et al. Involvement of activation-induced cytidine deaminase in skin cancer development. The Journal of clinical investigation. 2016;126(4):1367-82.
62. Leeman-Neill RJ, et al. Inhibition of EGFR-STAT3 signaling with erlotinib prevents carcinogenesis in a chemically-induced mouse model of oral squamous cell carcinoma. Cancer prevention research. 2011;4(2):230-7.
63. Schoop RA, et al. Apoptin induces apoptosis in an oral cancer mouse model. Cancer biology & therapy. 2008;7(9):1368-73.
64. Turnbull DH, et al. MRI in mouse developmental biology. An International Journal Devoted to the Development and Application of Magnetic Resonance In vivo. 2007;20(3):265-74.
65. McRobbie DW, et al. MRI from Picture to Proton: Cambridge university press; 2017.
66. Escors D, et al. Lentiviral vectors in gene therapy: their current status and future potential. Archivum immunologiae et therapiae experimentalis. 2010;58(2):107-19.
67. SM Wold W, et al. Adenovirus vectors for gene therapy, vaccination and cancer gene therapy. Current gene therapy. 2013;13(6):421-33.

68. Vannucci L, et al. Viral vectors: a look back and ahead on gene transfer technology. New Microbiol. 2013;36(1):1-22.
69. Schambach A, et al. Biosafety features of lentiviral vectors. 2013;24(2):132-42.
70. Ciuffi A. Mechanisms governing lentivirus integration site selection. 2008;8(6):419-29.
71. Liu BH, et al. CMV enhancer/human PDGF-β promoter for neuron-specific transgene expression. Gene therapy. 2004;11(1):52.
72. Byun H-M, et al. Plasmid vectors harboring cellular promoters can induce prolonged gene expression in hematopoietic and mesenchymal progenitor cells. Biochemical and biophysical research communications. 2005;332(2):518-23.
73. Kim S, et al. Efficiency of the elongation factor-1α promoter in mammalian embryonic stem cells using lentiviral gene delivery systems. Stem cells and development. 2007;16(4):537-46.
74. Nishihara E, et al. Treatment of thyroid carcinoma cells with four different suicide gene/prodrug combinations in vitro. Anticancer research. 1998;18(3A):1521-5.
75. Gambhir SS, et al. Imaging adenoviral-directed reporter gene expression in living animals with positron emission tomography. The National Academy of Sciences. 1999;96(5):2333-8.
76. De Wet JR, et al. Cloning of firefly luciferase cDNA and the expression of active luciferase in Escherichia coli. Proceedings of the National Academy of Sciences. 1985;82(23):7870-3.
77. De Wet JR, et al. Firefly luciferase gene: structure and expression in mammalian cells. Molecular and cellular biology. 1987;7(2):725-37.
78. Inc. NEB. Troubleshooting Guide for Cloning: New England BioLabs; 2019 [cited 2019 05/2]. Available from: https://www.neb.com/tools-and-resources/troubleshooting-guides/troubleshooting-guide-for-cloning.
79. Williams RJ. Restriction endonuclease. Molecular biotechnology. 2003;23(3):225-43.
80. Amessou M, et al. Targeting Intercellular Communication in Cancer Gene Therapy. Novel Gene Therapy Approaches: IntechOpen; 2013.
81. Matono S, et al. Bystander effect in suicide gene therapy is directly proportional to the degree of gap junctional intercellular communication in esophageal cancer. Oncology. 2003;23(5):1309-15.
82. Li S, et al. Connexin43-containing gap junctions potentiate extracellular Ca2+-induced odontoblastic differentiation of human dental pulp stem cells via Erk1/2. 2015;338(1):1-9.
83. Rajasekhar VK, et al. Regulatory networks in stem cells: Springer; 2009.
84. Brockmeyer P, et al. Membrane connexin 43 acts as an independent prognostic marker in oral squamous cell carcinoma. International journal of oncology. 2014;45(1):273-81.
85. Stewart WW. Functional connections between cells as revealed by dye-coupling with a highly fluorescent naphthalimide tracer. Cell. 1978;14(3):741-59.
86. El-Fouly MH, et al. Scrape-loading and dye transfer: a rapid and simple technique to study gap junctional intercellular communication. Experimental cell research. 1987;168(2):422-30.
87. Weber PA, et al. The permeability of gap junction channels to probes of different size is dependent on connexin composition and permeant-pore affinities. 2004;87(2):958-73.
88. Formigli L, et al. Morphofunctional integration between skeletal myoblasts and adult cardiomyocytes in coculture is favored by direct cell-cell contacts and relaxin treatment. American Journal of Physiology-Cell Physiology. 2005;288(4):C795-C804.
89. Jones C, et al. Dye-coupling compartments in the human eccrine sweat gland. American Journal of Physiology-Cell Physiology. 1989;256(3):C478-C85.
90. Belzer V, et al. Coupling among interstitial cells of Cajal in the human ileum. Neurogastroenterology & Motility. 2004;16(1):75-80.
91. Kisselbach L, et al. CD90 Expression on human primary cells and elimination of contaminating fibroblasts from cell cultures. Cytotechnology. 2009;59(1):31-44.
92. Inoue H, et al. A novel function of EpCAM in oral squamous cell carcinoma cells under anchorage-independent conditions. International journal of oncology. 2011;39(6):1401-5.
93. Sen S, et al. Expression of epithelial cell adhesion molecule (Ep CAM) in oral squamous cell carcinoma. Histopathology. 2016;68(6):897-904.
94. Halter M, et al. Automated live cell imaging of green fluorescent protein degradation in individual fibroblasts. Cytometry Part A: the journal of the International Society for Analytical Cytology. 2007;71(10):827-34.
95. Ribeiro DA, et al. Gingival changes in wistar rats after oral treatment with 4-nitroquinoline 1-oxide. European journal of dentistry. 2007;1(3):152.
96. Foy J-P, et al. The dynamics of gene expression changes in a mouse model of oral tumorigenesis may help refine prevention and treatment strategies in patients with oral cancer. Oncotarget. 2016;7(24):35932.
97. Czerninski R, et al. Targeting mammalian target of rapamycin by rapamycin prevents tumor progression in an oral-specific chemical carcinogenesis model. 2009;2(1):27-36.
98. Suzuki R, et al. An animal model for the rapid induction of tongue neoplasms in human c-Ha-ras proto-oncogene transgenic rats by 4-nitroquinoline 1-oxide: its potential use for preclinical chemoprevention studies. Carcinogenesis. 2005;27(3):619-30.

99. Chandolia B, et al. Can MMP-9 be a prognosticator marker for oral squamous cell carcinoma? Journal of clinical and diagnostic research: JCDR. 2016;10(1):ZC09.
100. Gnepp DR. Diagnostic Surgical Pathology of the Head and Neck: Expert Consult-Online and Print: Elsevier Health Sciences; 2009.
101. Sudhakara M, et al. Uncommon features in conventional oral squamous cell carcinoma. Journal of oral and maxillofacial pathology: JOMFP. 2016;20(2):316.
102. Essa AA, et al. Keratin pearl degradation in oral squamous cell carcinoma: reciprocal roles of neutrophils and macrophages. Journal of Oral Pathology & Medicine. 2014;43(10):778-84.
103. Kalele K, et al. Oral Squamous Cell Carcinoma: Hematoxylin and Eosin Staining. Journal of clinical and diagnostic research: JCDR. 2015;9(9):ZJ01.
104. Loro E, et al. In Vivo Evaluation of the Mechanical and Viscoelastic Properties of the Rat Tongue. JoVE (Journal of Visualized Experiments). 2017(125):e56006.
105. Chen X, et al. Double staining immunohistochemistry. North American journal of medical sciences. 2010;2(5):241.
106. Saghravanian N, et al. Expression of p63 and CD44 in oral squamous cell carcinoma and correlation with clinicopathological parameters. Archives of oral biology. 2017;82:160-5.
107. Missero C, et al. p63 in squamous cell carcinoma of the skin: more than a stem cell/progenitor marker. Journal of Investigative Dermatology. 2017;137(2):280-1.
108. Patel SB, et al. Immunohistochemical evaluation of p63 and cyclin D1 in oral squamous cell carcinoma and leukoplakia. Journal of oral and maxillofacial surgeons. 2017;43(5):324-30.
109. Chen C, et al. The biology and role of CD44 in cancer progression: therapeutic implications. Journal of hematology & oncology. 2018;11(1):64.
110. Wang SJ, et al. CD44 variant isoforms in head and neck squamous cell carcinoma progression. The Laryngoscope. 2009;119(8):1518-30.
111. Shimada Y, et al. Expression of podoplanin, CD44, and p63 in squamous cell carcinoma of the lung. Cancer science. 2009;100(11):2054-9.
112. Ries J, et al. Expression of melanoma-associated antigens in oral squamous cell carcinoma. Journal of oral pathology & medicine. 2008;37(2):88-93.
113. Montoro JRdMC, et al. Expression of cancer-testis antigens MAGE-A4 and MAGE-C1 in oral squamous cell carcinoma. Head & neck. 2012;34(8):1123-8.
114. Müller-Richter UD, et al. Analysis of expression profiles of MAGE-A antigens in oral squamous cell carcinoma cell lines. Head & face medicine. 2009;5(1):10.
115. Kocher T, et al. Identification and intracellular location of MAGE-3 gene product. Cancer Research. 1995;55(11):2236-9.
116. Koontongkaew S, et al. Alterations of p53, pRb, cyclin D1 and cdk4 in human oral and pharyngeal squamous cell carcinomas. Oral oncology. 2000;36(4):334-9.
117. Kerdpon D, et al. Expression of p53 in oral mucosal hyperplasia, dysplasia and squamous cell carcinoma. Oral diseases. 1997;3(2):86-92.
118. Shi S-R, et al. Antigen retrieval immunohistochemistry: future prospects in research and diagnosis over two decades. Journal of Histochemistry & Cytochemistry. 2011;59(1):13-32.
119. Xie S, et al. What is the prognostic significance of Ki-67 positivity in oral squamous cell carcinoma? Journal of Cancer. 2016;7(7):758.
120. Lothaire P, et al. Molecular markers of head and neck squamous cell carcinoma: promising signs in need of prospective evaluation. Head & Neck. 2006;28(3):256-69.
121. Shi S-R, et al. Antigen retrieval in formalin-fixed, paraffin-embedded tissues: an enhancement method for immunohistochemical staining based on microwave oven heating of tissue sections. Journal of Histochemistry & Cytochemistry. 1991;39(6):741-8.
122. Nauta JM, et al. Epithelial dysplasia and squamous cell carcinoma of the Wistar rat palatal mucosa: 4NQO model. Head & Neck. 1996;18(5):441-9.
123. Kaplan I, et al. PCNA in palate and tongue mucosal dysplastic lesions induced by topically applied 4NQO in desalivated rat. Medicina oral: organo oficial de la Sociedad Espanola de Medicina Oral y de la Academia Iberoamericana de Patologia y Medicina Bucal. 2002;7(5):336-43.
124. Abou-Madi N. Anesthesia and analgesia of small mammals. Recent Advances in Veterinary Anesthesia and Analgesia: Companion Animals International Veterinary Information. 2006.
125. Ohne M, et al. Tongue carcinoma of rats induced by oral administration of 4-nitroquinoline 1-oxide (4NQO) in drinking water. Oral surgery, medicine, pathology. 1985;59(6):600-7.
126. Nadaf A, et al. Analysis of the invasive edge in primary and secondary oral squamous cell carcinoma: An independent prognostic marker: A retrospective study. Journal of oral and maxillofacial pathology: JOMFP. 2016;20(2):239.
127. Tang X-H, et al. Oral cavity and esophageal carcinogenesis modeled in carcinogen-treated mice. Clinical Cancer Research. 2004;10(1):301-13.
128. Wallenius K, et al. Oral cancer in rats induced by the water-soluble carcinogen 4-nitrochinoline N-oxide. Odontologisk revy. 1973;24(1):39.

6 Supplemental information

6.1 Supplemental methods

6.1.1 Agarose gel electrophoresis

A 1% agarose (Invitrogen) gel was prepared employing Tris base, acetic acid and ethylenediaminetetraacetic acid (EDTA) 1x buffer (TAE 1x buffer; Sigma-Aldrich). A dilution of $1/10\,000$ Gelred® (Biotium, Brussels, Belgium) was added before letting the agarose gel solidify. Samples were loaded using Gel Loading Dye (6x; Thermo Scientific) and a 1 kb Plus DNA ladder (GeneRuler, ready-to-use; Thermo Scientific) was used to distinguish fragments. The agarose gel was allowed to run on 80 – 120 Volts before visualization. Agarose gels were visualized by the ultraviolet transilluminator (D-DiGit, Li-Cor, Leusden, The Netherlands).

6.1.2 Heavy antigen retrieval

Rat tongue slides were immersed in citrate buffer (pH 6) after deparaffination and heated for five minutes at maximum power. After two to three minutes, the power was bisected for the remainder of the heating step. Next, the buffer was repleted before slides were heated twice more for five minutes at half the maximal power with a two-minute cooling step in between each heating step. The slides were then left to rest in the citrate buffer for forty-five minutes before continuing with the immunohistochemical staining protocol.